energies

MDPI

Review

Combustion Chemistry of Unsaturated Hydrocarbons Mixed with NO_x: A Review with a Focus on Their Interactions

Ruoyue Tang [1] and Song Cheng [1,2,*]

[1] Department of Mechanical Engineering, The Hong Kong Polytechnic University, Kowloon 999077, Hong Kong
[2] Research Centre for Resources Engineering towards Carbon Neutrality, The Hong Kong Polytechnic University, Kowloon 999077, Hong Kong
* Correspondence: songryan.cheng@polyu.edu.hk

Abstract: Unsaturated hydrocarbons are major components of transportation fuels, combustion intermediates, and unburnt exhaust emissions. Conversely, NO_x species are minor species present in the residual and exhaust gases of gasoline-fueled engines and gas turbines. Their co-existence in transportation engines is quite common, particularly with exhaust gas recirculation, which can greatly influence engine combustion characteristics. Therefore, this paper presents a review on the combustion chemistry of unsaturated hydrocarbons and NO_x mixtures, with a focus on their chemical kinetic interactions. First, a comprehensive overview of fundamental combustion experiments is provided, covering mixtures of C_2–C_5 unsaturated/oxygenated species (namely alkenes, alkynes, dienes, alcohols, ethers, ketones, and furans) and three major NO_x species (namely NO, NO_2, and N_2O), as well as reactors including jet-stirred reactors, flow reactors, burners, shock tubes, and rapid compression machines. Then, two widely adopted nitrogen chemistry models are evaluated in conjunction with a core chemistry model (i.e., NUIGMech1.1) via detailed chemical kinetic modeling, and the model similarities and differences across broad temperature ranges are highlighted. Thereafter, the unique interconversions between the three major NO_x species are presented. In particular, the controversy regarding the pathways governing NO and NO_2 conversion is discussed. Following this, the key direct interaction reactions between unsaturated species and NO_x species are overviewed. Finally, the distinguishing features of the combustion chemistry for unsaturated hydrocarbon and NO_x mixtures are summarized, and recommendations for future research on this topic are highlighted.

Keywords: combustion chemistry; unsaturated hydrocarbon/NO_x mixture; fundamental combustion experiments; chemical kinetic modeling; interaction chemistry

Citation: Tang, R.; Cheng, S. Combustion Chemistry of Unsaturated Hydrocarbons Mixed with NO_x: A Review with a Focus on Their Interactions. *Energies* **2023**, *16*, 4967. https://doi.org/10.3390/en16134967

Academic Editor: Adonios Karpetis

Received: 24 May 2023
Revised: 22 June 2023
Accepted: 23 June 2023
Published: 26 June 2023

1. Introduction

Unsaturated hydrocarbons are organic compounds composed of carbon and hydrogen atoms, consisting of double or triple bonds between two adjacent carbon atoms. They are classified as olefins, alkynes, aromatics, etc., depending on the type of bond and molecular structure. These types of hydrocarbons are highly reactive and tend to undergo addition reactions with elemental halogens, hydrogen halides, alcohols, and many other compounds [1–3]. Unsaturated hydrocarbons usually form during the refining of crude oil to gasoline by cracking the heavier fractions, making up 15–20% of gasoline, which affects the octane number and the pollutant emissions of gasoline [4]. They also serve as potential fuels or propellants for novel propulsion systems. For instance, ethylene has been adopted as a scramjet fuel [5]. Furthermore, unsaturated hydrocarbons are the main intermediate products of alkane oxidation through H-atom abstraction reactions or cleavages of β C–H bonds in alkyl radicals [6,7] and a major component of unburnt exhaust hydrocarbons [8].

Conversely, nitrogen oxides are poisonous [9], highly reactive gases that are commonly produced during combustion processes. The primary mechanisms for the combustion-based production of NO_x include thermal NO_x, prompt NO_x, and fuel NO_x

production [10,11]. All three mechanisms of NO_x formation involve combustion-generated radicals or require a high temperature, producing NO, N_2O, and NO_2 as the main components. NO is a heteronuclear diatomic molecule (often considered a radical) possessing an unpaired electron, which contributes to its high reactivity and makes it easy to oxidize to produce NO_2. NO_2 also contains an unpaired electron, making it behave like a free radical. Due to this, hydrogen extraction reactions occur between NO_2 and saturated hydrocarbons, and addition reactions occur between NO_2 and unsaturated hydrocarbons or aromatic hydrocarbons. N_2O is a strong oxidant that can sustain combustion without the presence of oxygen under certain conditions [12]. It easily decomposes into nitrogen and oxygen at high temperatures, making it popular as a propellant component and in motor racing to increase engine power output [13].

The abundant co-existence of unsaturated hydrocarbons (e.g., from fuel constituents, combustion intermediates, and residual unburnt hydrocarbons) and NO_x species (e.g., from residue gas, recirculated exhaust gas, and combustion intermediates of nitrogen-containing fuels) in internal combustion engines has made it necessary to study their chemical kinetic interactions. These interactions can be influential, given the prominent impact of NO_x, particularly NO, on fuel autoignition and other combustion properties, as observed in both fundamental reactors [14,15] and practical engines [16,17]. However, past studies have almost all focused on the effects of blending NO_x species with saturated hydrocarbons, whereas blending with unsaturated hydrocarbons remains almost unexplored. On the other hand, it is also of particular interest to understand the chemical kinetics governing the unique interactions between NO_x species and unsaturated hydrocarbons. For instance, N_2O has been reported to bond directly to double carbon–carbon bonds, forming either a three-membered epoxide (C–O–C) or a five-membered heterocycle (C–N=N–O–C) that subsequently decomposes into ketones [18–20]. These unique and direct interactions have yet to be discussed consistently, let alone implemented in chemical kinetic models.

Therefore, this work aimed to review the existing studies on the combustion chemistry of oxygenated and unsaturated hydrocarbons mixed with NO_x species, with a focus on their chemical kinetic interactions. Firstly, we review fundamental combustion experiments conducted in rapid compression machines (RCMs), shock tubes, jet-stirred reactors (JSRs), flow reactors, and burners. Secondly, two widely recognized kinetic models, developed by Konnov et al. [21–23] and Glarborg et al. [24], are introduced and evaluated in conjunction with NUIGMech1.1 [25]. Thirdly, the conversion pathways between NO_x species are summarized. In particular, the conversions between NO and NO_2 are discussed in detail. Finally, the direct interaction reactions between unsaturated hydrocarbons and NO_x are highlighted and discussed.

2. Fundamental Combustion Experiments

Fundamental combustion experiments are highly valuable for understanding the fuel behavior and governing chemistry across wide ranges of thermodynamic and fuel-loading conditions that have been tailored to represent specific types of practical engines. Compared to data collected directly from practical engines, fundamental combustion experiments are more beneficial for establishing consistent comparisons across various research groups, owning to the small facility-to-facility differences associated with fundamental reactors. The experiments reviewed herein include speciation in flow reactors and JSRs, ignition delay time (IDT) measurements in shock tubes and RCMs, and laminar burning velocity (LBV) measurements in fundamental burners. Several kinds of species are considered, in the following order: alkenes, alkynes, oxygenates, and mixtures, arranged from lower to higher carbon numbers, i.e., C_1 to C_5. Figure 1 shows the number of papers published every decade related to fundamental combustion experiments on unsaturated and oxygenated hydrocarbon and NO_x mixtures, as reviewed in this work. It can be observed that this topic has received widespread attention since 1990, with more attention paid to N_2O.

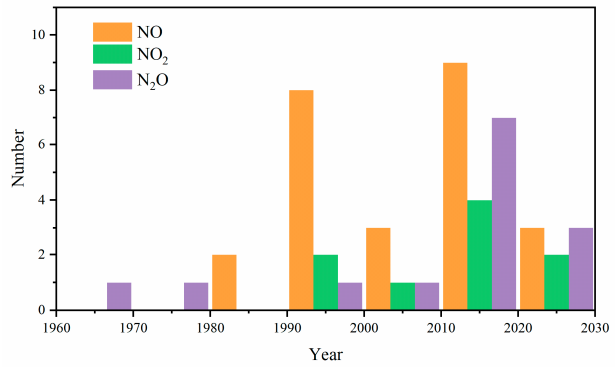

Figure 1. The number of papers related to experiments on unsaturated and oxygenated hydrocarbon and NO_x mixtures.

2.1. Unsaturated Hydrocarbons Mixed with NO

To date, most studies on the effects of blending NO_x with unsaturated hydrocarbons have focused on NO rather than NO_2 or N_2O. Among these studies, speciation in flow reactors is the most popular topic. All these studies are summarized in Table 1 and discussed briefly below.

The fundamental combustion of ethylene/NO mixtures has been studied by several researchers. Doughty et al. [26] first investigated the influence of NO addition on C_2H_4 oxidation at 650–1000 K in an atmospheric flow reactor. It was found that NO promoted the oxidation of C_2H_4 and the formation of formaldehyde under oxygen-rich conditions. The authors attributed this to C_2H_4 oxidation via OH addition as the initial step, with the production of OH radicals being promoted by NO addition. Dagaut et al. [27] studied the reduction of NO (1000 ppm) by C_2H_4 in a JSR at atmospheric pressure and temperatures ranging from 900 to 1400 K under fuel-lean to fuel-rich conditions (ϕ = 0.75–2.0) to reproduce a reburn situation, and additional fuel and oxidants were added at later stages to reduce the NO_x produced in the previous stage. The NO concentration profile showed that NO was easier to reduce at higher temperatures and under slightly fuel-rich conditions. A kinetic analysis was also performed, which showed that HCCO radicals played an important role in the reduction of NO by C_2H_4. Following this, Dagaut et al. [28] revisited the mutual sensitization between C_2H_4 and NO and between C_2H_6 and NO in a JSR at 700 to 1150 K and atmospheric pressure, and a detailed kinetic model was also developed. The authors emphasized the importance of NO conversion to NO_2 by HO_2, i.e., NO + HO_2 = NO_2+ OH, with NO to NO_2 conversion enhanced and fuel oxidation also promoted due to the generation of OH radicals. Gimenez-Lopez et al. [29] studied the interaction between C_2H_4 and NO (500 ppm) in another flow reactor under a high pressure of 60 bar and low-to-intermediate temperatures (600–900 K). It was observed that the presence of NO shifted the onset of the oxidation of C_2H_4 to lower temperatures, indicating the promoting effect of NO on C_2H_4 oxidation.

Propene has attracted wide attention in the past few decades, as it is considered a key soot precursor. As such, there have also been several studies on the fundamental combustion properties of propene/NO mixtures. Atakan and Hartlieb [30] measured the NO concentration in fuel-rich (ϕ = 1.5, 1.8, 2.3) C_3H_6 flames with 0.2–1% NO seeded into premixed gas to study the reburning of NO with C_3H_6. They attributed NO consumption to the different radicals and reactions in the flame zone, among which HCCO radicals were the most significant compared to CH and C radicals. Dagaut et al. [31] investigated the reduction of NO by C_3H_6 in a JSR at 1 atm and 1100–1450 K. As shown in Figure 2, NO reduction was favored at higher temperatures and under fuel-rich conditions, which was consistent with the trends observed for C_2H_4 [27]. The reduction of NO resulted in the simultaneous production of HCN, which increased and then decreased as the temperature increased. Yuan et al. [32] investigated C_3H_6 oxidation with NO/NO_2 doping under fuel-lean to fuel-rich conditions in a flow reactor coupled with synchrotron vacuum

ultraviolet photoionization mass spectrometry. Though only NO was added initially, part of the NO was believed to have been converted to NO_2. Therefore, the change in C_3H_6 oxidation was attributed to the combined effect of NO and NO_2. It was found that NO/NO_2 addition enhanced the reactivity of C_3H_6, which could be attributed to the reaction of allyl radicals with NO_2, promoting the production of C_3H_5O. This then decomposed to acrolein and H atoms, forming a reactive chain sequence and hence leading to remarkable low-temperature reactivity.

Table 1. Literature studies on fundamental combustion experiments involving unsaturated hydrocarbons mixed with NO.

Author	Mixture	Experimental Device	Properties	Conditions
Doughty et al. [26]	Ethylene (C_2H_4)/NO/O_2/N_2	Flow reactor	Speciation	T = 650–1000 K P = 1 atm τ = 2–3.5 s NO: 0–200 ppm
Dagaut et al. [27]	Ethylene (C_2H_4)/NO /O_2/N_2	Jet-stirred reactor	Speciation	T = 900–1400 K P = 1 atm ϕ = 0.75–2 τ = 0.12–0.16 s NO: 1000 ppm
Dagaut et al. [28]	Ethylene (C_2H_4) /Ethane (C_2H_6)/NO/O_2/N_2	Jet-stirred reactor	Speciation	T = 700–1150 K P = 1 atm τ = 0.12–0.24 s NO: 0–1200 ppm
Gimenez-Lopez et al. [29]	Ethylene (C_2H_4)/NO/O_2/N_2	Flow reactor	Speciation	T = 600–900 K P = 60 bar τ (s) = 8892/T NO: 500 ppm
Atakan and Hartlieb [30]	Propene (C_3H_6)/NO/O_2/Ar	Burner	Speciation	T = 313 K ϕ = 1.5, 1.8, 2.3 NO: 0.2–1%
Dagaut et al. [31]	Propene (C_3H_6)/NO/O_2/N_2	Jet-stirred reactor	Speciation	T = 1100–1450 K P = 1 atm ϕ = 0.75–2 τ = 0.12–0.16 s NO: 750–1000 ppm
Yuan et al. [32]	Propene (C_3H_6)/NO/NO_2/O_2	Flow reactor	Speciation	T = 725–1250 K P = 1 bar]ϕ = 0.23, 1.35 τ = 0.3–0.5 s NO_x: 0.3%
Gossler et al. [33]	i-Butene (i-C_4H_8)/ 1-butene (1-C_4H_8)/ NO/O_2/Ar	Flow reactor	Speciation	T = 600–1200 K P = 1 atm ϕ = 2 τ = 0.6–1.4 s NO: 1000 ppm
Prabhu et al. [34]	1-Pentene (1-C_5H_{10})/NO/O_2/N_2	Flow reactor	Speciation	T = 600–800 K P = 6 atm ϕ = 0.4 τ = 30–220 ms NO: 0–500 ppm
Quang and Vanpee [35]	Acetylene (C_2H_2)/NO	Circular flat burner	Speciation	T = 297 K P = 80 torr NO: 73.1%, 83.3%

Table 1. *Cont.*

Author	Mixture	Experimental Device	Properties	Conditions
Quang and Vanpee [36]	Acetylene (C_2H_2)/NO	Circular flat burner	Speciation	T = 2800–3100 K P = 80 torr NO: 73.1%, 83.3%
Dagaut et al. [37]	Acetylene (C_2H_2)/NO/O_2/N_2	Jet-stirred reactor	Speciation	T = 1050–1300 K P = 1 atm ϕ = 0.75–2 τ = 0.12–0.16 s NO: 1000 ppm
Guarneri et al. [38]	Furan (C4H4O)/NO/O_2/Ar	Shock tube	Speciation	T = 1210–1950 K P = 12.4–15.3 atm ϕ = 2.4–5.0 τ = 570–1140 µs NO: 300–380 ppm
Alexandrino et al. [39]	2,5-Dimethylfuran (2,5-DMF)/NO/O_2/N_2	Flow reactor	Speciation	T = 800–1400 K P = 1 atm]ϕ = 0.03–3.3 τ (s) = 195/T NO: 900 ppm
Alexandrino et al. [40]	2-methylfuran (2-MF)/NO/O_2/N_2	Flow reactor	Speciation	T = 800–1400 K P = 1 atm ϕ = 0.02–3.3 τ (s) = 195/T NO: 900 ppm
Alzueta et al. [41]	Acetone (CH_3COCH_3)/NO/O_2/H_2O/N_2	Flow reactor	Speciation	T = 700–1500 K P = 1 atm ϕ = 0.14–2.9 τ (s) = 400/T NO: 290 ppm, 300 ppm
Williams and Pasternack [42]	Methane (CH_4)/acetylene (C_2H_2)/ethylene (C_2H_4)/ethane (C_2H_6)/NO/O_2/N_2	McKenna flat flame burner	Speciation	T (peak) = 1800 K P = 10 torr ϕ = 1 NO: 1%
Garborg et al. [43]	Acetylene (C_2H_2)/ethylene (C_2H_4)/NO/O_2/N_2	Flow reactor	Speciation	T = 800–1500 K P = 1.05 atm ϕ = 1.3 τ (s) = 162/T NO: 835 ppm ϕ = 1.5 τ (s) = 165/T NO: 790 ppm
Konnov et al. [44]	Ethylene (C_2H_4)/ethane (C_2H_6)/propane (C_3H_8)/NO/O_2/N_2	Burner	LBV, speciation	T = 298 K P = 1 atm]ϕ = 0.6–1.8 NO: 100 ppm
Hori et al. [45]	Methane (CH_4)/ethylene (C_2H_4)/ethane (C_2H_6)/ propene (C_3H_6)/propane (C_3H_8)/NO/O_2/N_2	Flow reactor	Speciation	T = 600–1100 K P = 1 atm τ = 0.16–1.46 s NO: 20 ppm

Table 1. *Cont.*

Author	Mixture	Experimental Device	Properties	Conditions
Abian et al. [46]	Acetylene (C_2H_2)/ethanol (C_2H_5OH)/NO/O_2/N_2/H_2O	Flow reactor	Speciation	T = 775–1375 K P = 1 atm ϕ = 0.5–5 τ (s) = 195/T NO: 100, 500, 1200 ppm
Marrodan et al. [47]	Dimethyl ether (DME)/ acetylene (C_2H_2)/NO/O_2/N_2/H_2O	Flow reactor	Speciation	T = 575–1475 K P = 1 atm ϕ = 0.05–5 τ (s) = 195/T NO: 500 ppm
Cheng et al. [48]	Surrogate/EGR/ethylene (C_2H_4)/propene (C_3H_6)/ i-butene (i-C_4H_8)/NO/O_2/N_2	Rapid compression machine	IDT	T = 680–950 K P = 20, 40 bar ϕ = 1 NO: 70 ppm

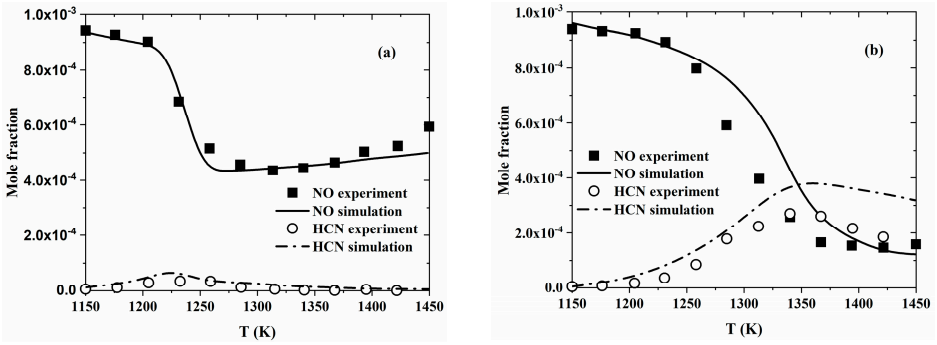

Figure 2. Comparison between experimental data (symbols) and modeling results (lines) with regard to the reduction of NO (1000 ppm) by C_3H_6 in a flow reactor at 1 atm and (**a**) ϕ = 1.0 or (**b**) ϕ = 1.5 [31].

Many studies have also focused on larger alkenes, though these are much scarcer than studies on ethylene and propene, as shown in Table 1. The oxidation of 1-butene and i-butene with NO (1000 ppm) in a flow reactor under fuel-rich conditions (ϕ = 2.0) was investigated by Gossler et al. [33] at a temperature range of 600–1200 K and atmospheric pressure using both experimental and modeling frameworks. The results are presented in Figure 3, showing that NO promoted fuel consumption due to the contribution of NO to the radical pool; for example, NO + HO_2 = NO_2 + OH and CH_3 + NO_2 = CH_3O + NO. Furthermore, NO addition also enhanced the negative temperature coefficient (NTC) behavior of i-butene. These trends were attributed to the competition between chain propagation and chain termination reactions among the i-C_4H_7 + NO_2 → products. Prabhu et al. [34] measured species profiles during the oxidation of 1-C_5H_{10} with 0–500 ppm NO doped in a flow reactor at 600–800 K and under a higher pressure and lean conditions, namely 6 atm and ϕ = 0.4, respectively. A small amount of NO altered the 1-C_5H_{10} oxidation reactivity at all temperatures. Whether the influence of NO caused promotion or inhibition depended on the competition between the promoting reaction with HO_2 radicals (NO + HO_2 = NO_2 + OH) and the inhibiting reaction with OH radicals (NO + OH + M = HONO + M, where M represents a third body).

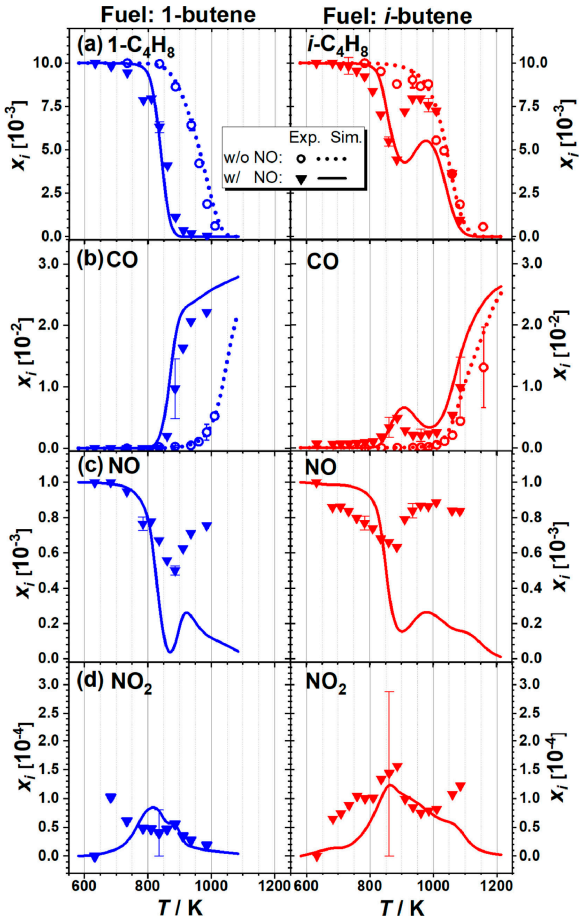

Figure 3. Experimental (symbols) and modeled (lines) mole fraction profiles during the oxidation of 1-C_4H_8 and i-C_4H_8 with and without NO (1000 ppm) in a JSR at ϕ = 2 and P = 1 atm: (**a**) 1-C_4H_8, i-C_4H_8; (**b**) CO; (**c**) NO; (**d**) NO_2 [33].

Studies of alkynes have mainly focused on C_2H_2. Quang and Vanpee [35] detected the free radicals, e.g., CN, NH, CH, C_2, and OH, in fuel-rich (C_2H_2: 26.9%, NO: 73.1%) and stoichiometric (C_2H_2: 16.7%, NO: 83.3%) C_2H_2/NO flames at 80 torr by spectrography. The results suggested that CH and C_2 were excited thermally with CN and NH as the chemiluminescent origins. Later, these researchers [36] measured the concentration of radicals and stable products in a C_2H_2/NO flame under both fuel-rich (C_2H_2: 26.9%, NO: 73.1%) and stoichiometric (C_2H_2: 16.7%, NO: 83.3%) conditions in the temperature range of 2800–3100 K. It was observed that NO was mainly consumed by the previously detected free radicals, e.g., C_2, CH, CN, and NH, and the consumption process was rather fast. Dagaut et al. [37] also explored the reduction of NO by C_2H_2 in a JSR operating at 1 atm and temperatures from 1050 to 1300 K under equivalence ratios of 0.75–2.0 to simulate the reburning zone. The reduction of NO by acetylene corroborated the results observed for C_2H_4 [27] and C_3H_6 [31], indicating that there might be a universal interaction mechanism between unsaturated hydrocarbons and NO.

In addition, efforts have been made to explore the effect of NO on the oxidation of oxygenated species. Guarneri et al. [38] investigated NO reduction with furan in a shock tube under pyrolytic and oxidative conditions covering the temperature range of 1210–1950 K, pressures from 12.4 to 15.3 atm, residence times of 570–1140 μs, and initial NO concentrations of 300–380 ppm. It was found that the starting points of the reduction of NO by furan shifted to lower temperatures when the equivalence ratio decreased. Alexandrino et al. [39] studied the oxidation of 2,5-dimethylfuran (2,5-DMF) with NO (900 ppm) addition in an isothermal quartz flow reactor at atmospheric pressure in the temperature range of 800–1400 K. Temperature, stoichiometry, and 2,5-DMF concentration were

found to influence the NO conversion rate considerably. Only under fuel-lean conditions did the presence of NO lower the onset temperature of 2,5-DMF oxidation. Given that 2-methylfuran (2-MF) is an important intermediate during 2,5-DMF oxidation, Alexandrino et al. [40] further carried out experiments in the same flow reactor to investigate the oxidation of 2-MF in the absence and presence of NO at temperatures of 800–1400 K and equivalence ratios of 0.02–3.3, and the NO concentration (900 ppm) was much higher than the 2-MF concentration (100 ppm). Due to the higher amount of OH radicals produced by NO via reaction with HO_2, the onset temperature of 2-MF oxidation shifted to lower temperatures when NO was added. Alzueta et al. [41] explored acetone oxidation with and without NO (290 ppm, 300 ppm) in a flow reactor for a temperature range of 700–1500 K and equivalence ratios of 0.14–2.9. The experiments indicated that NO did not exhibit significant impacts on the oxidation of acetone while interacting with the acetone derivatives, primarily CH_3 and HCCO.

Unsaturated hydrocarbons have also been studied as components of fuel blends. Williams and Pasternack [42] studied NO (1%) reactivity in CH_4, C_2H_6, C_2H_4, and C_2H_2 flames by comparing the radical profiles, i.e., CH, OH, NO, CN, NCO, NH, and metastable-state $^3C_2$, using a McKenna flat flame burner at 10 torr and under stoichiometric conditions. The profiles indicated that the concentrations of nitrogen-containing radicals were quite similar in the CH_4, C_2H_6, and C_2H_4 flames and reached the highest values in the C_2H_2 flame, indicating that more NO was converted to nitrogen-containing radicals and the reactivity of NO was the highest in the C_2H_2 flame. Glarborg et al. [43] studied the reduction of NO by C_2H_4 and C_2H_2 in a flow reactor at 800–1500 K and 1.05 atm, adopting the same flow reactor for CH_4 and C_2H_6 as in [49] for comparison. HCCO + NO → products and CH_3 + NO → products were identified as the most important interaction pathways for NO reduction. Konnov et al. [44] measured the LBV and NO concentrations in the post-flame zone of C_2H_4, C_2H_6, and C_3H_8 flames with NO addition (100 ppm in N_2) at equivalence ratios of 0.6–1.8 and atmospheric pressure. NO conversion was reported in all three flames. However, NO addition did not lead to any noticeable change in LBV. Hori et al. [45] studied the influence of several hydrocarbons (50 ppm), including CH_4, C_2H_4, C_2H_6, C_3H_6, and C_3H_8, on NO (20 ppm) conversion in a flow reactor at residence times ranging from 0.16 to 1.46 s and temperatures ranging from 600 to 1100 K. The experimental results indicated that C_2H_4 and C_3H_8 effectively converted NO to NO_2, while CH_4 showed the poorest ability to convert NO. The authors concluded that HO_2, instead of RO_2, was the most dominant radical in converting NO to NO_2. Abian et al. [46] carried out flow reactor experiments at atmospheric pressure and 775–1375 K to study the influence of C_2H_2 and C_2H_5OH mixtures on NO reduction. It was found that the addition of C_2H_5OH shifted the onset of NO reduction to higher temperatures, while the highest NO conversion ratio remained constant. The authors reported that the initial concentrations of NO and oxygen were key factors in the NO reduction. Marrodan et al. [47] investigated the oxidation of dimethyl ether (DME) and acetylene mixtures doped with NO (500 ppm) in a flow reactor. Greater NO conversion occurred with the absence of DME in fuel-rich and stoichiometric conditions. Cheng et al. [48] studied the influence of olefins, including C_2H_4, C_3H_6, and i-C_4H_8, on gasoline surrogate autoignition with the presence of NO (70 ppm) at pressures of 20 and 40 bar and temperatures ranging from 680 to 950 K in an RCM. The results, as shown in Figure 4, indicated that the addition of NO promoted the autoignition reactivity of the surrogate at all temperatures and pressures, while olefin additions seemingly diminished the promoting effect of NO, making the mixture less reactive. Through sensitivity and rate-of-production analyses, the authors found that olefins and their derivatives could interact with NO_x species directly, which was particularly pronounced with propene and i-butene addition. This led to increased ignition reactivity by facilitating NO production, which subsequently caused increased OH production.

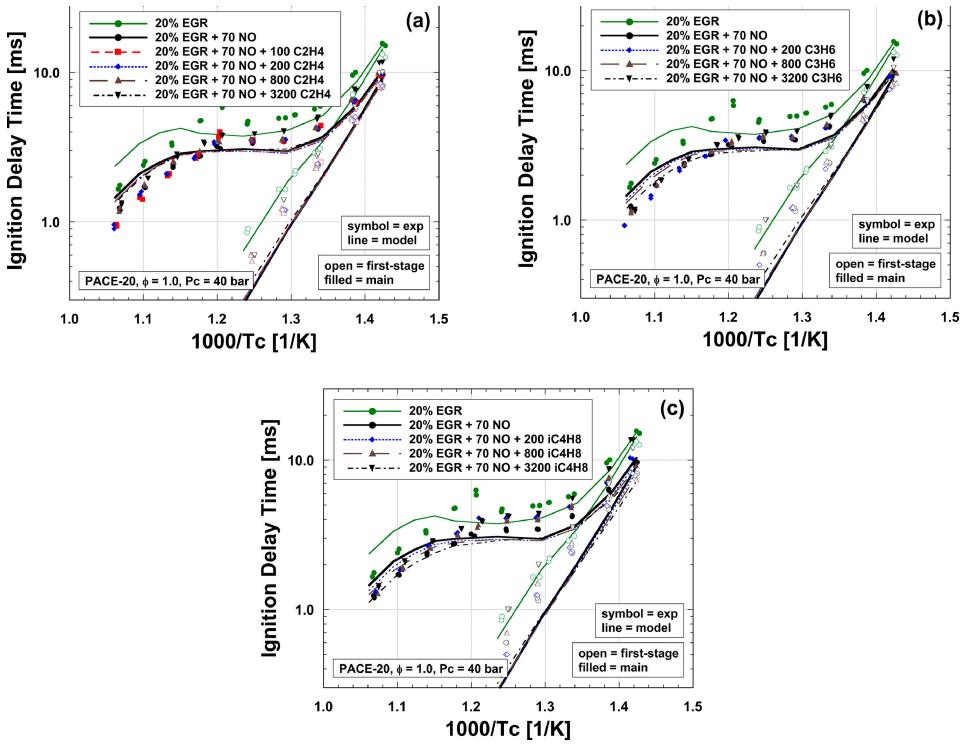

Figure 4. Experimental (lines) and simulated (symbols) IDTs of surrogate with 20% EGR; 70 ppm NO; and different olefin concentrations (0, 100, 200, 800, and 3200 ppm) at 40 bar and ϕ = 1: (**a**) C_2H_4, (**b**) C_3H_6, (**c**) i-C_4H_8 [48].

In general, NO addition improves the reactivity of unsaturated hydrocarbons at low temperatures, which manifests in the shortening of the IDT and a reduction in the onset temperature of oxidation.

2.2. Unsaturated Hydrocarbons Mixed with NO_2

Compared with NO, experimental studies on unsaturated hydrocarbons with NO_2 have been scarcer, with most focusing on ethylene for alkenes and acetylene for alkynes. These studies are summarized in Table 2.

Abian et al. [50] studied the effect of NO_x addition on soot formation by carrying out C_2H_4 pyrolysis experiments with NO, NO_2, and N_2O addition in a flow reactor at atmospheric pressure and in the 975–1475 K temperature range. The measurements indicated that NO_2 had the strongest impact in reducing the production of soot, while N_2O displayed the smallest impact. The authors attributed the inhibiting effect of NO_2 to the ability of NO_2 to form NO and OH through the reaction $NO_2 + H = OH + NO$, which in turn were involved in reburn and oxidation reactions, leading to the consumption of soot precursors, e.g., C_2H_2 and C_2H_4. Menon et al. [51] studied a laminar premixed C_2H_4/air flame with and without NO_2 addition (5% by volume) at equivalence ratios of 2.34 and 2.64 to investigate the influence of NO_2 on soot formation. NO_2 was observed to be effective at reducing the soot volume fraction and delaying the onset of soot formation as a function of the height above the burner. This was attributed to the fast reaction between H atoms and NO_2 and the reduction in the carbon flux to the soot precursor by radicals, e.g., OH and O, produced by the aforementioned reaction. Deng et al. [52] measured the IDT of $C_2H_4/NO_2/O_2/Ar$ mixtures in a shock tube at pressures of 1.2–10 atm, temperatures of 920–1780 K, and equivalence ratios of 0.5–2.0. The addition of NO_2 (0.5%) promoted the reactivity of C_2H_4, leading to shortened IDTs, particularly at higher pressures and lower temperatures and under fuel-rich conditions.

Table 2. Literature studies on fundamental combustion experiments involving unsaturated hydrocarbons with NO_2.

Author	Mixture	Experimental Device	Properties	Conditions
Abian et al. [50]	Ethylene $(C_2H_4)/NO/NO_2/N_2O/N_2$	Flow reactor	Speciation	T = 975–1475 K P = 1 atm τ (s) = 4550/T NO: 590–12,200 ppm NO_2: 500–11,800 ppm N_2O: 480–11,900 ppm
Menon et al. [51]	Ethylene $(C_2H_4)/NO_2/air/N_2$	Burner	Speciation, soot volume fraction	P = 1 atm ϕ = 2.34, 2.64 NO_2: 5% by volume
Deng et al. [52]	Ethylene $(C_2H_4)/NO_2/O_2/Ar$	Shock tube	IDT	T = 920–1780 K P = 1.2–10 atm]ϕ = 0.5–2.0 NO_2: 0.5%
Volponi and Branch [53]	Acetylene $(C_2H_2)/NO_2/O_2/Ar$	Flat flame burner	Speciation	P = 25 torr
Marshall et al. [54]	Acetylene $(C_2H_2)/O_2/NO_2/NO$	Flow reactor	Speciation	T = 600–900 K P = 50–60 bar ϕ = 0.05, 1.0, 5.6 NO/NO_2: 500 ppm
Jin et al. [55]	Ethanol $(C_2H_5OH)/NO_2/O_2/Ar$	Shock tube	IDT	T = 1050–1650 K P = 0.2 MPa]ϕ = 0.5–1.5 NO_2: 0.2%, 1%
Ye et al. [56]	Dimethyl ether (DME)/$NO_2/O_2/Ar$	Shock tube	IDT	T = 987–1517 K P = 4, 10 atm ϕ = 0.5, 1.0, 2.0 NO_2: 0.201%, 1.722%
Alzueta et al. [57]	Dimethyl ether (DME)/$NO_2/O_2/H_2O/N_2$	Flow reactor	Speciation	T = 600–1500 K P = 1 atm ϕ = 0.013–2.04 τ (s) $\approx$ 188/T NO: 493 ppm, 502 ppm, 508 ppm NO_2: 43 ppm, 44 ppm, 72 ppm

Volponi and Branch [53] studied the structure of laminar premixed flames for $C_2H_2/O_2/Ar$ and $C_2H_2/NO_2/Ar$ mixtures. The LBV of the $C_2H_2/N_2O/Ar$ mixture was found to be much lower than that of the $C_2H_2/O_2/Ar$ mixture. The addition of NO_2 was also found to change the CO to CO_2 conversion rate. Marshall et al. [54] investigated C_2H_2 oxidation with NO_2 and NO addition at high pressures (50–60 bar) in a flow reactor. The C_2H_2 mole fraction profiles at three equivalence ratios (namely 0.05, 1.0, and 5.6) were recorded. The results indicated that NO_x addition had promotion and inhibition effects at low (e.g., <750 K) and high (e.g., >750 K) temperatures, respectively, with the opposite effects being the most prominent under fuel-rich conditions, as illustrated in Figure 5. It was confirmed that the direct interaction between C_2H_2 and NO_2 forming CHOCHON was responsible for the promoting effect of NO_2 at low temperatures, which subsequently decomposed to form triplet carbene CHCHO (:C(H)CHO) and NO.

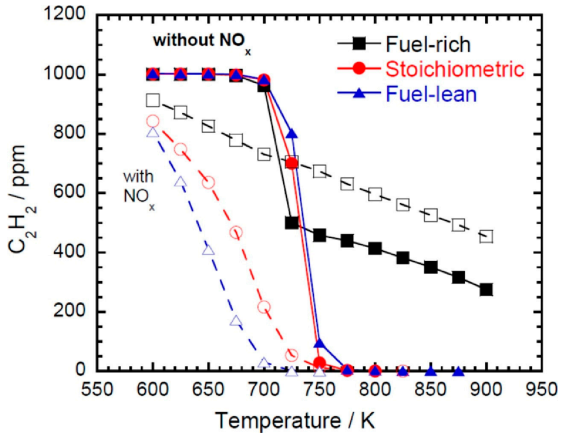

Figure 5. Comparison of measured concentration profiles for acetylene under different stoichiometry conditions (ϕ = 5.6/59.6 bar; ϕ = 1/59.6 bar; and ϕ = 0.05/49.6 bar) with (open symbols) and without (solid symbols) NO_x [54].

Jin et al. [55] investigated the impact of NO_2 on C_2H_5OH autoignition in a shock tube at a pressure of 0.20 MPa; a temperature range of 1050–1650 K; equivalence ratios of 0.5, 1.0, and 1.5; and C_2H_5OH/NO_2 mixing ratios of 100/0, 90/10, and 50/50. The IDT of C_2H_5OH decreased with the addition of NO_2 under all equivalence ratios studied, indicating the promoting effect of NO_2 on the ethanol autoignition reactivity. The authors attributed this to the enrichment of the OH radical pool by NO_2. Ye et al. [56] measured the IDTs of $DME/NO_2/Ar/O_2$ mixtures in a shock tube at 4 and 10 atm and equivalence ratios of 0.5–2.0. Seeding NO_2 shortened the IDT of DME, and the effect was enhanced with an increased NO_2 concentration. Alzueta et al. [57] also studied the impact of NO (493 ppm, 502 ppm, and 508 ppm) and NO_2 (43 ppm, 44 ppm, and 72 ppm) on DME oxidation in a flow reactor at atmospheric pressure, a temperature range of 600–1500 K, and equivalence ratios of 0.013–2.04. It was observed that both NO and NO_2 shifted the start of DME oxidation to lower temperatures by promoting H atom production through the following reactions: $CH_3 + NO_2 = CH_3O + NO$ and $CH_3O = CH_2O + H$.

Several researchers have also studied the reaction of NO_2 with other organics, e.g., dialkenes and conjugated alkenes. Atkinson et al. [58] determined the rate coefficients of reactions of NO_2 with several organic species at 295 K, including 2-methyl-2-butene, 2,3-dimethyl-2-butene, 1,3-butadiene, 2-methyl-1,3-butadiene, cyclohexene, 1,3-cyclohexadiene, 1,4-cyclohexadiene, 1,3-cycloheptadiene, α-pinene, β-pinene, Δ^3-carene, d-limonene, α-terpinene, γ-terpinene, α-phellandrene, toluene, and crotonaldehyde. Bernard et al. [59] investigated the reaction between conjugated alkenes (isoprene, myrcene, ocimene, and 1,3-cyclohexadiene) and NO_2 at 298 K and atmospheric pressure. The rate coefficients of these reactions were determined, and the main products were also identified. Ohta et al. [60] also determined the rate coefficients for 16 kinds of conjugated alkenes reacting with NO_2, e.g., cis-1,3-pentadiene, trans-1,3-pentadiene, 2-methyl-1,3-butadiene. It was found that due to the difference in the activation energy, the rate coefficients for conjugated alkenes were much larger than the rate coefficients for mono-alkenes. It is worth noting that several studies have proposed that dialkenes promote the conversion of NO to NO_2 [61,62]. The dialkene first reacts with NO_2 to form a free radical. Then, a peroxy species forms via O_2 addition, which further reacts with NO to form NO_2. In this way, NO is converted to NO_2 easily and quickly. This is a notable channel for not only the interaction between dialkenes and NO_x but also NO_x conversion.

Similarly to NO addition, the presence of NO_2 usually shortens the IDT and shifts the start of oxidation to lower temperatures, promoting the reactivity of oxygenated and unsaturated hydrocarbons at a low temperature range.

2.3. Unsaturated Hydrocarbons Mixed with N_2O

Most works on the combustion characteristics of unsaturated hydrocarbons and N_2O mixtures have been carried out to explore the performance of nitrous oxide fuel blend propellants. The unsaturated hydrocarbons investigated so far are light hydrocarbons, e.g., C_2H_2 and C_2H_4, whereas studies on their heavier counterparts are seriously lacking. These studies are summarized in Table 3.

Table 3. Literature studies on fundamental combustion experiments involving unsaturated hydrocarbons with N_2O.

Author	Mixture	Experimental Device	Properties	Conditions
Trenwith [63]	Ethylene (C_2H_4)/N_2O	Cylindrical silica vessel	Speciation	T = 828–875 K P = 20–100 mm
Howard et al. [64]	Ethylene (C_2H_4)/N_2O/Ar	McKenna flat flame burner	Speciation	P = 20 torr
Werling et al. [65]	Ethylene (C_2H_4)/N_2O	Ignition chamber	Flame propagation, flashback behavior	T = 293 K P = 1–1.75 bar
Naumann et al. [66]	Ethylene (C_2H_4)/N_2O/N_2	Shock tube	IDT	T = 1050–2000 K P = 1, 4, 16 bar N_2O: 17.14% ϕ = 1.0
	Ethylene (C_2H_4)/N_2O/N_2	Burner	LBV	T = 473 K P = 1–10 bar ϕ = 1.0 N_2O: 42.86%
Kick et al. [67]	Ethylene (C_2H_4)/N_2O/N_2/Ar/CO	Shock tube	IDT	T = 1050–2000 K P = 1, 4, 16 bar ϕ = 1.0 N_2O: 17.14%, 42.86%
	Ethylene (C_2H_4)/N_2O/N_2	Burner	LBV	T = 473 K P = 1, 3, 6 bar ϕ = 1.0 N_2O: 42.86%
Deng et al. [68]	Ethylene (C_2H_4)/N_2O/N_2/Ar	Shock tube	IDT	T = 1090–1760 K P = 1.2–10 atm]ϕ = 0.5–2.0 N_2O: 3–12%
Zhang et al. [69]	Ethylene (C_2H_4)/N_2O/Ar	Rapid compression machine	IDT	T = 885–940 K P = 2.5–4.3 MPa ϕ = 1.05–1.35 N_2O: 40.8%, 42.5%
Yang et al. [70]	Ethylene (C_2H_4)/N_2O/Ar	Rapid compression machine	IDT	T = 1170–1290 K P = 15–45 bar ϕ = 0.5–2 N_2O: 1.5%, 3%
Wang and Zhang [71]	Ethylene (C_2H_4)/N_2O/Ar	Steel cube chamber	LBV	T = 280 K P = 0.5–2.0 atm ϕ = 0.2–2.4
Aldous et al. [72]	Acetylene (C_2H_2)/N_2O	Bunsen burner	LBV	T = 400/500/600 K P = 1 atm ϕ = 0.35–2.0
Alekseev et al. [73]	Acetylene (C_2H_2)/N_2O/Ar	Shock tube	Oxygen atom profiles	T = 1688–3179 K P = 1.8–3.0 bar N_2O: 10 ppm

Table 3. *Cont.*

Author	Mixture	Experimental Device	Properties	Conditions
Powell et al. [74]	Hydrogen (H_2)/methane (CH_4)/acetylene (C_2H_2)/propane (C_3H_8)/ N_2O/N_2	McKenna flat flame burner	LBV	T = 295 K P = 0.8 atm ϕ = 0.56–1.6
Powell and Papas [75]	methane (CH_4)/acetylene (C_2H_2)/propane (C_3H_8)/ N_2O/N_2	McKenna flat flame burner	NO concentration profiles	P = 0.81 atm ϕ = 1.0 N_2O: 31.34% (CH_4) N_2O: 24.71% (C_2H_2) N_2O: 32.88% (C_3H_8)
Mevel and Shepherd [76]	Methane (CH_4)/ethane (C_2H_6)/ethylene (C_2H_4)/ acetylene (C_2H_2)/O_2/N_2O/Ar	Shock tube	IDT	T = 1269–1945 K P = 222–397 kPa ϕ = 0.78–1.80 N_2O: 1.133–3.598%

Unlike the situation for hydrocarbons with NO and NO_2, where O_2 is always the oxidizer, N_2O can be regarded as the oxidizer when O_2 is absent. Trenwith [63] measured the primary products from C_2H_4 oxidation by N_2O at low pressures of 20–100 mmHg and temperatures between 828 and 875 K. Nitrogen, carbon monoxide, methane, ethane, a small amount of acetaldehyde, hydrogen, and hydrocarbons of high molecular weight were detected. Howard et al. [64] applied molecular beam mass spectrometry with a triple quadrupole mass spectrometer to determine the species concentration of free radicals in a C_2H_4/N_2O/Ar flame. Radicals, e.g., H, O, and OH, and stable species, e.g., N_2, CO, NO, CO_2, O_2, and H_2O, were detected.

The German Aerospace Center (DLR) has made great efforts to further the understanding of the combustion characteristics of nitrous oxide fuel blend propellants. Werling et al. [65] conducted C_2H_4/N_2O ignition experiments in a cylindrical, optically accessible ignition chamber and characterized the LBV and flame flashback behavior. Naumann et al. [66] measured the IDT of a C_2H_4/N_2O mixture with 80% dilution by N_2 in a shock tube and the LBV of a C_2H_4/N_2O mixture with 50% dilution by N_2 in a high-pressure burner system. In a subsequent study, they further measured the IDT of a C_2H_4/N_2O mixture with different dilution gases, including N_2, CO_2, and Ar, at different dilution ratios [67]. It was observed that the IDT of the mixture was shorter under a higher pressure, and the LBV was the highest at 1 bar. To establish a comparison between unsaturated and saturated hydrocarbons, the IDTs of $C_2H_6/N_2O/N_2$ mixtures and $C_2H_6/O_2/N_2$ mixtures were further measured behind reflected shock waves by Naumann et al. [77]. Comparisons across three different pressure values are shown in Figure 6, indicating that C_2H_4 became more reactive than C_2H_6 with the presence of N_2O, particularly at lower temperatures and higher pressures.

Deng et al. [68] performed shock tube experiments to measure the IDTs of $C_2H_4/N_2O/O_2$/Ar mixtures with different ratios of $N_2O/(N_2O + O_2)$ (0, 50, 80, and 100%) at pressures ranging from 1.2 to 10 atm and temperatures ranging from 1090 to 1760 K. The results indicated that the IDT increased obviously with an increase in the $N_2O/(N_2O + O_2)$ ratio. N_2O unimolecular decomposition, forming N_2 and O, and reactions between N_2O and H, forming N_2 and OH, were proved to be more important than the interaction between N_2O and C_2H_4. Zhang et al. [69] measured the IDTs of N_2O/C_2H_4 propellants at 885–940 K, pressures of 2.5–4.3 MPa, and equivalence ratios of 1.05 and 1.35 in an RCM. A linearly fitted correlation was proposed to predict the IDTs of the N_2O/C_2H_4 propellants. It was also revealed that N_2O unimolecular decomposition was dominant at high temperatures, while N_2O and hydrocarbon interactions were dominant at low

temperatures. The autoignition boundary temperatures of Ar-diluted C_2H_4/N_2O mixtures were determined by Yang et al. [70] in an RCM at pressures of 15–45 bar and equivalence ratios of 0.5–2.0. The results showed that the boundary temperature became lower when the pressure, Ar dilution level, and fuel/oxidizer ratio increased. Wang and Zhang [71] determined the LBVs of C_2H_4/N_2O mixtures using spherical expansion flames at 0.5–2.0 atm. As shown in Figure 7, the LBVs of $C_2H_4/N_2O/N_2$ mixtures were found to be much smaller than those of $C_2H_4/O_2/N_2$ mixtures, particularly under near-stoichiometric conditions. Furthermore, the addition of N_2O to the C_2H_4/air mixture slightly increased the LBV. It was also found that the LBV of the C_2H_4/N_2O mixture was insensitive to pressure. The N_2O unimolecular decomposition reaction was also determined to be crucial in the C_2H_4/N_2O flame.

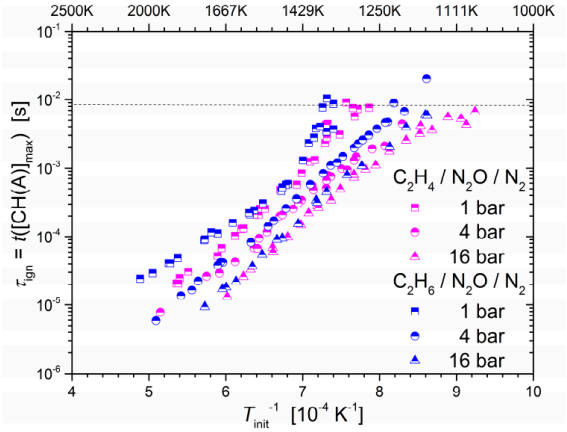

Figure 6. Measured IDTs of stoichiometric $C_2H_4/N_2O/N_2$ and $C_2H_6/N_2O/N_2$ mixtures diluted with nitrogen ((fuel + N_2O):N_2 = 1:5) at initial pressures of 1, 4, and 16 bar [63].

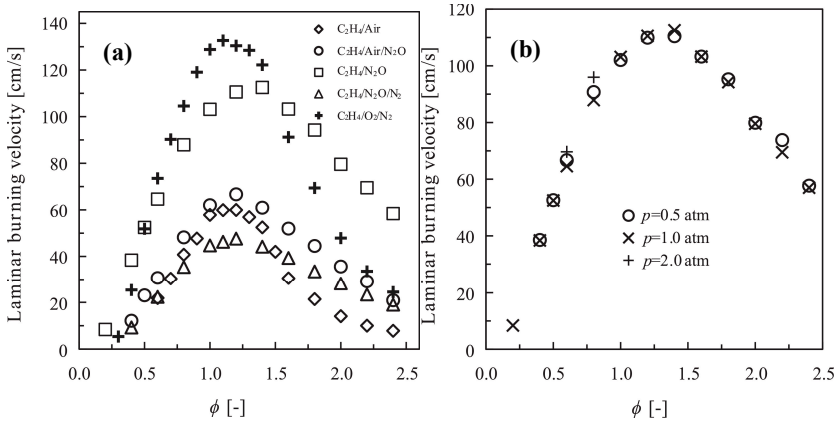

Figure 7. (**a**) The LBV of different mixtures at 1 atm and 280 K, (**b**) the effect of pressure on the LBV of a C_2H_4/N_2O mixture at 280 K [71].

There have only been a few studies on the fundamental combustion characteristics of C_2H_2/N_2O mixtures. As early as 1972, Aldous et al. [72] measured the LBVs of C_2H_2/N_2O mixtures in a Bunsen burner to provide suggestions for burner design. It was only recently that Alekseev et al. [73] recorded the oxygen atom concentration profile for an Ar-diluted C_2H_2/N_2O mixture based on shock waves at high temperatures from 1688 K to 3179 K. The O atom concentration increased with an increasing temperature, due to earlier N_2O decomposition at higher temperatures.

In addition to the work on C_2H_2 and C_2H_4, there have also been a few studies on the effects of N_2O addition on hydrocarbon mixtures containing C_2H_2 or/and C_2H_4. The LBVs of H_2, CH_4, C_2H_2, and C_3H_8 blended with N_2O were determined by Powell et al. [74] in a

McKenna flat flame burner at 0.8 atm and equivalence ratios of 0.58–1.6. The authors reported that the most sensitive reactions occurred within the hydrogen/N_2O sub-chemistry, and $N_2O + H = OH + N_2$ was proved to be critical in LBV determination. Later, Powell and Papas [75] measured the NO profiles in premixed CH_4/N_2O, C_2H_2/N_2O, and C_3H_8/N_2O flames with N_2 dilution under stoichiometric conditions at 0.81 atm. They found that the maximum NO concentrations in the three flames were quite similar. Mevel and Shepherd [76] conducted shock tube experiments for mixtures of N_2O and small hydrocarbons, including CH_4, C_2H_6, C_2H_4, C_2H_2, and their blends, both with and without O_2 at temperatures of 1269–1945 K, pressures of 222–397 kPa, and equivalence ratios of 0.78–1.80. The results indicated that the absence of O_2 dramatically reduced the IDTs. The ignition was found to be driven by $N_2O(+M) = N_2 + O(+M)$ and $N_2O + H = N_2 + OH$ with only N_2O as an oxidizer, while it was driven by $N_2O(+M) = N_2 + O(+M)$ and $H + O_2 = OH + O$ with both O_2 and N_2O present.

It has been found that when only N_2O is the oxidant, the reactivity of mixtures is much lower than in the presence of O_2, as indicated by the much longer IDT and lower LBV.

3. Chemical Kinetics

3.1. Widely Adopted Kinetic Models for Nitrogen Chemistry

The combustion research community has witnessed dramatic advances in chemical kinetic modeling over the past few decades, thanks to the development of chemical kinetic models and multi-scale chemical kinetic solvers. To date, several chemical kinetic models have already been developed, validated, and improved to a large extent for both unsaturated hydrocarbon and nitrogen chemistry. Kinetic models for unsaturated hydrocarbons have already been reviewed by Zhou et al. [6]; hence, these will not be discussed in this study. Among the kinetic models for nitrogen chemistry, the models of Konnov et al. [21–23] and Glarborg et al. [24] have been widely adopted. These models are therefore reviewed in this section.

The first version of Konnov's model [21] was released in 2000 and referred to as "Release 0.5". This was a detailed C/N/H/O model for C_1–C_6 hydrocarbons, consisting of 1200 reactions and 127 species. Since the release of this model, it has been widely validated against fundamental combustion experiments (including the LBV, IDT, and species profiles) for various hydrocarbons, including hydrogen, carbon monoxide, formaldehyde, methanol, methane, ethane, and propane. For instance, Konnov et al. [44] compared simulation results acquired using Release 0.5 with measured LBV and NO concentration profiles in a C_2H_4 flame with and without NO seeded at 1 atm and 298 K. The model reproduced the trends of the experiments, including the quantitative dependence of the LBV on the equivalence ratio and the minor impact of NO addition on the LBV, as shown in Figure 8. The model was also able to capture the qualitative trends in the post-flame NO concentration both with and without NO doping, as shown in Figure 9. Similarly to the model performance for CH_4, as reported in [22], the model showed divergence from the experimental results in Figure 9, consistently overpredicting and underpredicting the post-flame NO concentrations, respectively.

Although Release 0.5 performed reasonably well, an inadequacy in NO prediction still existed. Therefore, a modified version, named Release 0.6, was proposed by Konnov [23]. The modified model aimed to improve the performance of the original model in prompt NO formation. Thus, most reactions and thermodynamic data related to hydrocarbon oxidation and hydrogen sub-mechanisms remained unchanged. To achieve this goal, two new species (NCN and HNCN) were added, and three reactions ($CH + N_2 = HCN + N$, $CN + N_2O = CNN + NO$, and $CN + NCO = CNN + CO$) were removed and replaced by $CH + N_2 = NCN + H$, $CN + N_2O = NCN + NO$, and $CN + NCO = NCN + CO$ respectively, since NCN instead of CNN was proved to be crucial in the prompt NO route [78,79]. Furthermore, several reactions related to NCN and HNCN were added, and their rate coefficients were mainly adopted from the work of Lin et al. [80,81]. A comparison between the Release

0.5 model and the Release 0.6 model was performed, with both models used to simulate the NO concentration at 10 mm downstream from the flame front in $C_2H_4/O_2/N_2$ mixtures. Though there were nearly no changes in model performance under fuel-lean conditions, the performance of Release 0.6 improved greatly, particularly in predicting NO formation under fuel-rich conditions and all dilution ratios for premixed C_2H_4 flames, as can be seen from Figure 10. These improvements highlighted the important role of NCN and the related reactions in NO formation.

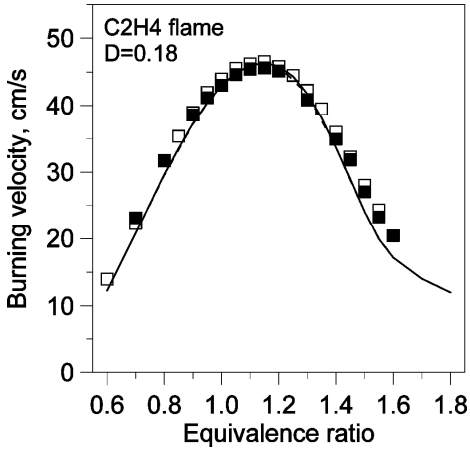

Figure 8. Adiabatic burning velocities of C_2H_4+ O_2 + N_2 flames doped with NO and without NO at 1 atm and a temperature of 298 K, D = $O_2/(O_2 + N_2)$ [44]. Empty symbols: measurements without NO; filled symbols: measurements with NO. Solid lines: modeling results with NO; dashed lines: modeling results without NO.

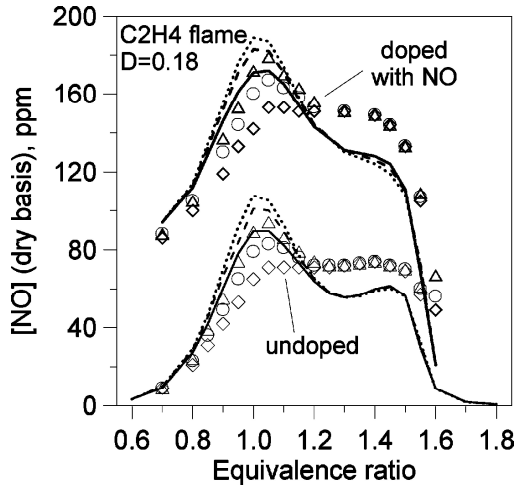

Figure 9. Concentration of NO at different distances from the burner in the post-flame zone of $C_2H_4/O_2/N_2$ flames with and without NO, D = $O_2/(O_2 + N_2)$ [44]. Lines: modeling; symbols: experiment. Solid lines and diamonds: [NO] at 10 mm from the burner surface; dashed lines and circles: [NO] at 15 mm; short-dashed lines and triangles: [NO] at 20 mm.

Many groups have used Konnov's model as an individual kinetic model or a sub-chemistry model (e.g., nitrogen sub-chemistry) to understand the combustion characteristics of hydrocarbon/NO_x mixtures. Powell and Papas [75] compared modeling results obtained using the Release 0.6 model with experimental results in the form of NO concentration profiles measured in premixed C_2H_2/N_2O flames. The comparison indicated that the model showed good performance in capturing NO profiles in a premixed C_2H_2/N_2O flame, as shown in Figure 11.

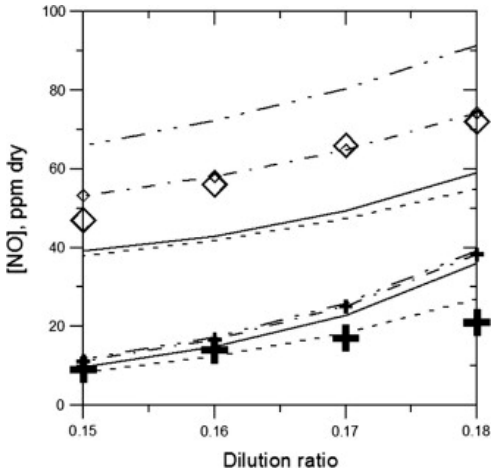

Figure 10. Concentration of NO produced by $C_2H_4/O_2/N_2$ mixtures under different dilution ratios [23]. Crosses: experimental results for ϕ = 0.8; diamonds: experimental results for ϕ = 1.3. Dashed lines with small symbols: simulation using Release 0.6; solid line: simulation using Release 0.5.

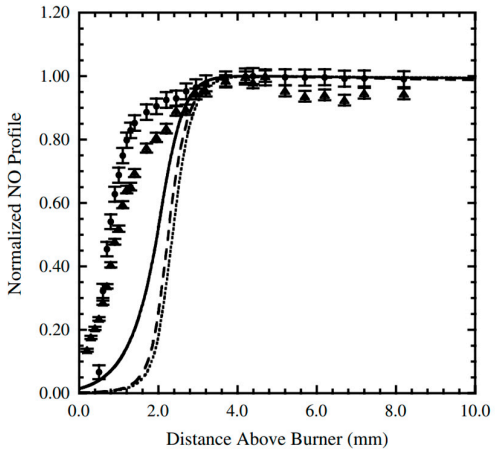

Figure 11. Experimental and modeled normalized NO profiles in premixed C_2H_2/N_2O flame [75]. •: experimental LIF data using Q1 (26:5) transition; ▲: experimental LIF data using Q1 (22:5) transition; dashed lines: predictions using the Release 0.6 model [23]; solid lines: predictions using the PPD mechanism.

The model developed by Glarborg et al. (referred to as the Glarborg model in the following) [24] included the sub-chemistries for hydrocarbons and nitrogen-containing species and the interacting chemistry between small hydrocarbons (e.g., CH_4) and nitrogen-containing species. It was developed based on previous studies on C_1–C_2 hydrocarbons [82–84], amines [85], cyanides [86], and hydrocarbon/nitrogen interactions [43,87,88]. Since its release, the model has been widely adopted to simulate ammonia combustion and NO_x formation in different combustion processes, and it has been demonstrated to have good predictive ability.

For instance, the Glarborg model was validated against the flow reactor experiments conducted by Alzueta et al. [43,49] for C_2H_2/NO and C_2H_4/NO mixtures. It was found that the production and consumption of HCN could be well predicted by the model. The NO reduction profiles were also reproduced by the model for C_2H_2/NO, and C_2H_4/NO mixtures, as shown in Figure 12.

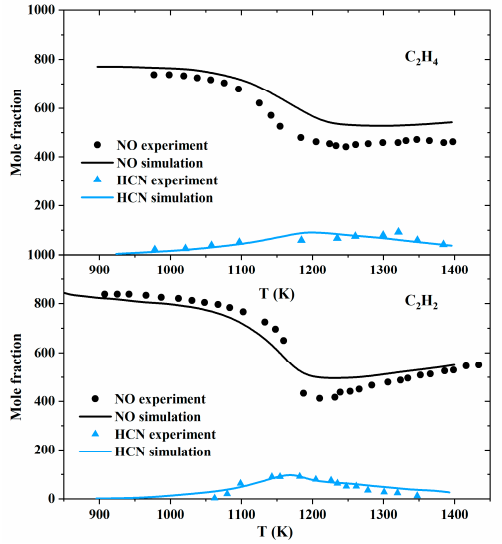

Figure 12. Comparison between experimental data and modeling predictions for the reduction of NO by hydrocarbons under reburning conditions in a quartz flow reactor [24]. Inlet concentrations: C_2H_2 = 890 ppm, O_2 = 1700 ppm, NO = 835 ppm (t = 162[K]/T); C_2H_4 = 1020 ppm, O_2 = 2015 ppm, NO = 790 ppm (t = 165[K]/T). All experiments were conducted with 2% H_2O, balanced N_2, and 1.05 atm. Symbols denote experimental data, while solid lines denote modeling predictions.

The Glarborg model has been widely adopted by other researchers for its nitrogen-related components to study the hydrocarbon interactions with nitrogen-containing species. Yuan et al. [32] considered the NO_x reactions and the interactions of NO_x with C_0–C_2 species provided by the Glarborg model and the C_3H_6 chemistry provided by the AramcoMech 3.0 model [89] to simulate measured species profiles during C_3H_6 oxidation with and without NO_x at atmospheric pressure in the temperature range of 725–1250 K, with excellent agreement observed (c.f., Figure 13).

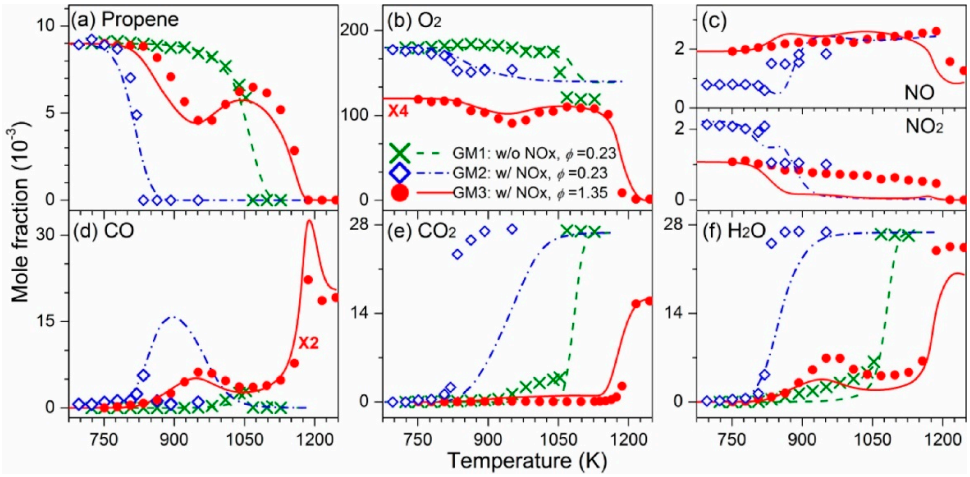

Figure 13. Experimental (symbols) and simulated (lines) mole fraction profiles of reactants and major products during the oxidation of C_3H_6 at 1 bar and φ = 0.23 (GM1, C_3H_6/O_2 mixture); φ = 0.23 (GM2, $C_3H_6/O_2/NO_x$ mixture); and φ = 1.35 (GM3, $C_3H_6/O_2/NO_x$ mixture). (**a**) C_3H_6, (**b**) O_2, (**c**) NO (upper panel) and NO_2 (lower panel), (**d**) CO, (**e**) CO_2, (**f**) H_2O [32].

To compare the performance of the Konnov model with that of the Glarborg model in predicting the combustion characteristics of unsaturated hydrocarbons and NO_x mixtures, they were merged with the NUIGMech1.1 model [25] developed by Curran et al., which included detailed C_1–C_7 hydrocarbon chemistry. The two merged models are marked as "Glarbog" and "Konnov", respectively, in Figures 14–18. The fundamental combustion

experiments at low to high temperatures for unsaturated hydrocarbons mixed with NO, NO_2, and N_2O, as reviewed in Section 2.1, were adopted for model comparison.

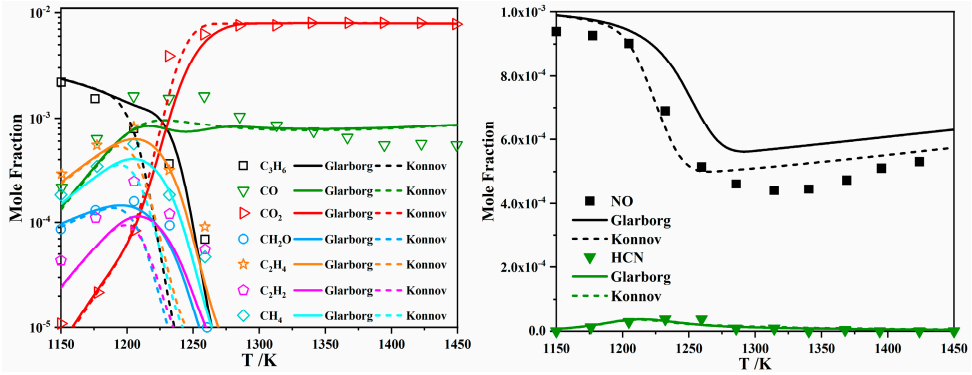

Figure 14. Comparison between experimental data (symbols) and modeling (lines) of NO (1000 ppm) reduction by C_3H_6 (2930 ppm) at an equivalence ratio of 1 and 1 atm [31].

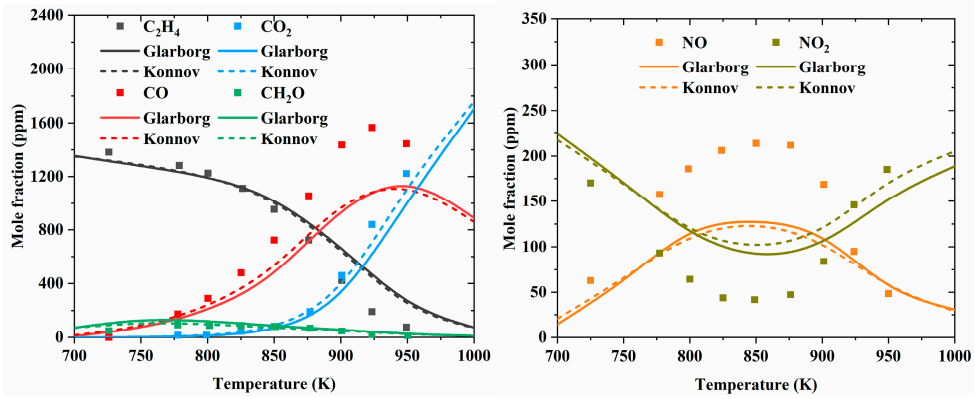

Figure 15. Comparison of experimental (symbols) and predicted (lines) concentration profiles for a $C_2H_4/O_2/NO/N_2$ mixture under fuel-lean conditions, t = 120 ms. Inlet composition: 1400 ppm C_2H_4, 37,500 ppm O_2, 240 ppm NO [28].

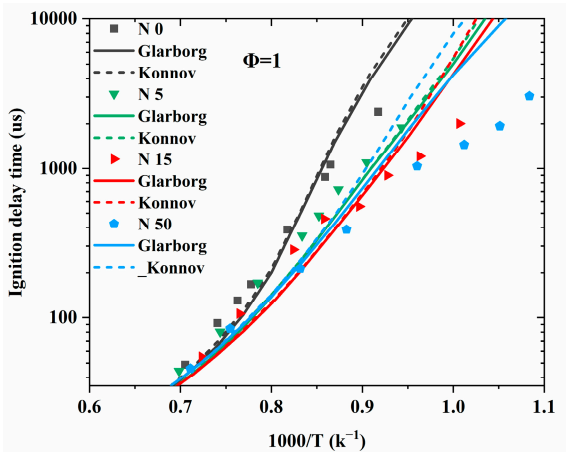

Figure 16. Ignition delay time comparison between the measurements (symbols) and simulations (lines) at an equivalence ratio of 1 and pressure of 10 atm. N0, N5, N15, and N50 represent an NO_2 concentration of 0%, 5%, 15%, and 50%, respectively, as a mole fraction of the C_2H_4 [52].

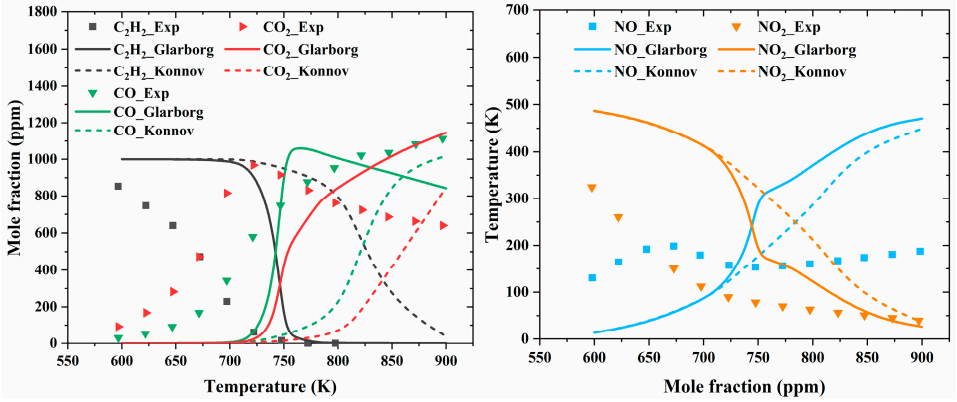

Figure 17. Comparison of experimental (symbols) and predicted (lines) concentration profiles as a function of the reactor temperature for the stoichiometric experiment with a $C_2H_2/O_2/NO_x/N_2$ mixture [54]. The reactor temperature profile was obtained from [29].

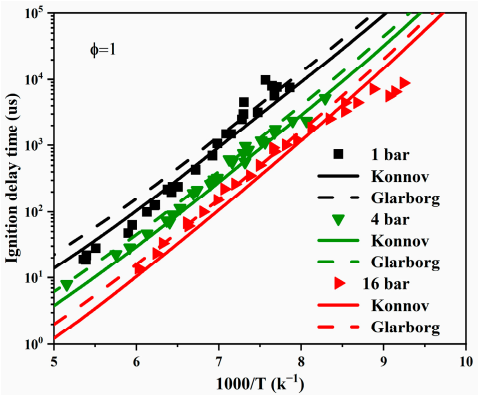

Figure 18. The experimental (symbols) and simulated (lines) IDTs for 20% (C_2H_4/N_2O) + 80% N_2 at an equivalence ratio of 1 and a pressure of 1 bar [77].

Figure 14 summarizes the simulated species profiles, along with the experimental results reported in [31], during C_3H_6 oxidation at 1150–1450 K in a JSR with 750–1000 ppm NO addition. Overall, the Konnov model agreed better with the experiments in terms of the NO profile, while the Glarborg model performed better in capturing the concentration profiles for C_3H_6, C_2H_4, C_2H_2, CH_2O, CH_4, CO_2, and CO. It is also obvious that the two models exhibited different reactivity levels, with the Konnov model predicting earlier fuel oxidation. The simulated and measured species profiles (adopted from [28]) during the oxidation of a $C_2H_4/O_2/NO/N_2$ mixture at lower temperatures (700–950 K) are shown in Figure 15. Similar simulation results were observed for the two models, which both underpredicted fuel consumption and NO formation. The poor model performance in replicating NO and NO_2 profiles is concerning, indicating that further investigations are needed. Further analysis indicated that $NO + HO_2 = NO_2 + OH$ and $ROO + NO = RO + NO_2$ are important interactions between hydrocarbons and NO_x, as elaborated by other studies [27,28,32,34]. The former converts fewer reactive HO_2 radicals into highly reactive OH radicals at low to intermediate temperatures, thereby promoting the mixture reactivity. The latter represents a direct interaction between hydrocarbons and NO_x, which converts ROO radicals into RO radicals, thereby shifting the reaction pathways away from OH branching. These reactions will be discussed in detail in Section 3.3.

Figure 16 shows the simulated IDTs using the Konnov and Glarborg models for a $C_2H_4/O_2/NO_2/N_2$ mixture, along with the experimental measurements obtained from a shock tube at 920–1780 K and 10 atm [52]. As can be seen from Figure 16, both models captured the promotion effect of NO_2 only at low addition levels. When the NO_2 concentration was above 15%, both models showed large discrepancies with the experiments and

failed to replicate the qualitative trends in the NO_2 addition effect. Although the simulation results using these two models were very similar, the Glarborg model showed better performance when the NO_2 addition was 50%. Figure 17 shows the comparison between the experimental results [54] and simulation results for a $C_2H_2/O_2/NO/NO_2/N_2$ mixture in a flow reactor at lower temperatures (600–900 K). It is obvious that both models performed unsatisfactorily in replicating the experiments, with better performance observed for the Glarborg model. In addition, at lower temperatures, the two models differed greatly from each other, in contrast to the trends observed in Figure 16.

Figure 18 shows the simulated and measured IDTs of a C_2H_4/N_2O mixture in a shock tube [77] within a high temperature regime and at three different pressures. In general, the Konnov model performed better than the Glarborg model, though the difference between the two models was small and could be complicated by experimental measurement uncertainties. Additionally, both models captured the pressure dependence commendably.

3.2. Conversion between NO_x Species

It has so far been established that NO_x species can easily convert between each other. This is most prominent between NO and NO_2 when O_2 is present, which has been observed in many studies. For instance, Yuan et al. [32] initially introduced $C_3H_6/O_2/NO$ gas mixtures into a flow reactor. However, part of the NO converted to NO_2 in the premixed pipeline (at room temperature) before entering the reactor. Thus, the NO/NO_2 ratio was determined at the inlet of the flow reactor using mass spectrometry. Similarly, in a shock tube study [90], NO was injected into the mixing tank to ensure fast mixing, and the final mixture of $n\text{-}C_7H_{16}/O_2/Ar/NO$ was allowed to equilibrate for 10 min before being injected into the shock tube driven section. After equilibrium, over half of the NO was converted to NO_2. These conversions have made interpreting NO_x blending effects particularly challenging. Therefore, this section aims to review the conversion pathways between NO_x species.

In most nitrogen chemistry models, the one-step conversion pathways between the three NO_x species can be summarized as shown in Figure 19. Specifically, N_2O reacts with H and O to form NO, via $N_2O + O = NO + NO$ and $N_2O + H = NO + NH$, respectively. Early in 1956, Kaufman et al. [91] measured the rate of decomposition of N_2O and the rate of formation of NO and then determined the rate of $N_2O + O = NO + NO$ theoretically. Baber and Dean [92] conducted shock tube experiments for the dissociation of N_2O/Ar mixtures over a temperature range of 1850–2540 K and proposed the rate coefficient of $N_2O + O = NO + NO$ by fitting the experimental results using a complex mechanism. Recently, Buczko et al. [93] re-evaluated the rate coefficient of $N_2O + O = NO + NO$ based on direct rate coefficient measurements and theoretical calculations. With the re-evaluated rate, thermal NO formation was accurately predicted. The rate coefficients mentioned above are plotted in Figure 20; it was found that the rate coefficient provided by Buczko et al. [93] was about an order of magnitude larger than that of Baber and Dean [92].

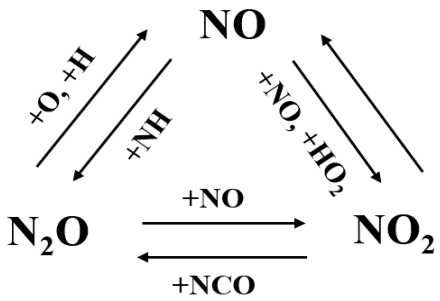

Figure 19. One-step conversion pathways between the three major NO_x species.

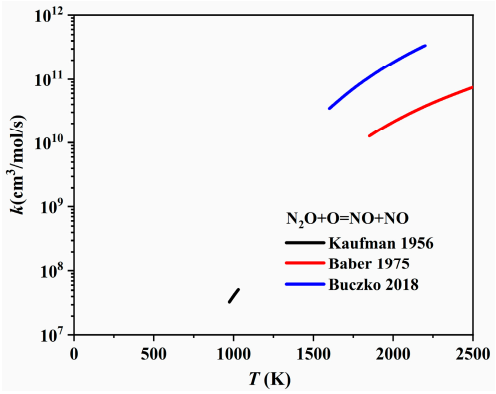

Figure 20. The rate coefficients of N_2O + O = NO + NO proposed by Kaufman et al. [91], Baber and Dean [92], and Buczko et al. [93].

As for the second N_2O to NO conversion reaction (N_2O + H = NO + NH), Baldwin et al. [94] first recommended a rate coefficient at 863 K by studying the reaction between H_2 and N_2O. Then, Marshall et al. [95] measured the rate coefficient for N_2O + H → products using high-temperature photochemistry. They also proposed a maximum rate coefficient for the N_2O + H = NO + NH channel at temperatures up to 2000 K. Bozzelli et al. [96] re-evaluated both the forward and reverse reaction rate coefficients of N_2O + H = NO + NH using experimental and theoretical data from the literature. As shown in Figure 21, the rate coefficients provided by Marshall et al. [95] and Bozzelli et al. [96] were quite similar. However, the rate coefficient offered by Baldwin et al. [94] at 837 K was much higher than that of both the abovementioned studies. The NO + NH = N_2O + H channel is responsible for the one-step conversion from NO to N_2O, as shown in Figure 19, which is also the reverse reaction of N_2O + H = NO + NH. Several studies have made further efforts to determine the rate coefficient of NO + NH = N_2O + H. For instance, Roose et al. [97] determined the rate coefficient for this reaction in a shock tube by measuring species concentrations, e.g., NO, NH_2, and NH, over the temperature range of 1780–2850 K. Kovacs et al. [98] optimized the Arrhenius parameters of NO + NH = N_2O + H by fitting the reaction rate against direct and indirect experiments with lower uncertainty. The rate coefficients provided by Bozzelli et al. [96], Roose et al. [97], and Kovacs et al. [98] are compared and presented in Figure 22. It is shown that the rate coefficients proposed by Bozzelli et al. [96] and Kovacs et al. [98] increased with the temperature increase, while the rate coefficient proposed by Roose et al. [97] demonstrated a contrary trend, decreasing with the temperature increase.

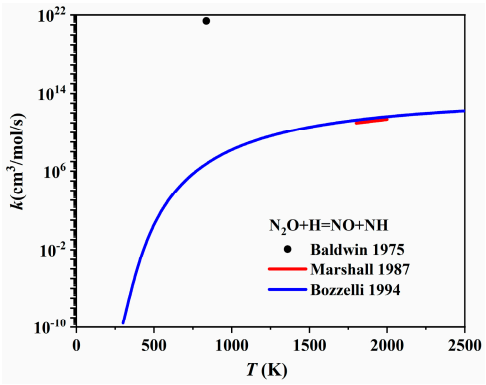

Figure 21. The rate coefficients of N_2O + H = NO + NH proposed by Baldwin et al. [94], Marshall et al. [95], and Bozzelli et al. [96].

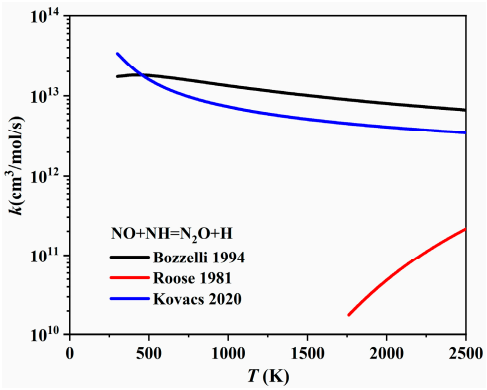

Figure 22. The rate coefficients of NO + NH = N_2O + H proposed by Bozzelli et al. [96], Roose et al. [97], and Kovacs et al. [98].

The one-step conversion pathways between N_2O and NO_2, i.e., NO_2 + NCO = N_2O + CO_2 and N_2O + NO = NO_2 + N_2, have been included in most nitrogen chemistries. The isocyanate radical, NCO, involved in the first pathway is a key intermediate during the rapid reduction of nitrogen oxides. Park and Hershberger [99] experimentally determined the rate coefficient of NO_2 + NCO → product channels using infrared diode laser absorption spectroscopy and found that N_2O and CO_2 accounted for over 90% of the products. Zhao et al. [100] conducted ab initio calculations for NO_2 + NCO = N_2O + CO_2 and determined the rate coefficients for the temperature range of 300–4000 K using transition state theory with correction for anharmonicity effects. As shown in Figure 23, the rate coefficient proposed by Park and Hershberger [99] was much larger than the rate coefficient calculated by Zhao et al. [100] at 296 K. The reaction rate of the second pathway (i.e., N_2O + NO = NO_2 + N_2) has always been determined during N_2O decomposition investigations. Kuafman and Kelso [101] determined the expression rate for N_2O + NO = NO_2 + N_2 over a low temperature range of 924–1030 K from concentration profiles measured after mixing NO and N_2O in a spherical quartz vessel. Later, Fishburne and Edse [102] extended the understanding of this reaction to a higher temperature range, i.e., 1500–2200 K, by measuring the rate of the thermal decomposition of N_2O in a shock tube. Mebel et al. [103] performed ab initio calculations, and the calculated rate coefficients were in close agreement with the earlier estimates of Hanson and Salimian [104]. These rate coefficients are plotted in Figure 24, appearing very similar.

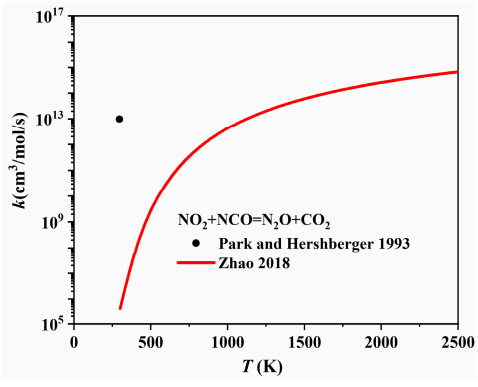

Figure 23. The rate coefficients of NO + NCO = N_2O + CO_2 proposed by Park and Hershberger [99] and Zhao et al. [100].

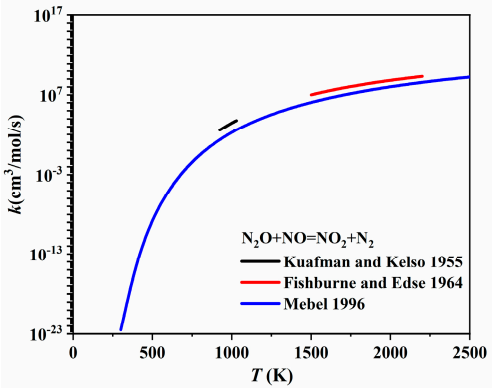

Figure 24. The rate coefficients of $N_2O + NO = NO_2 + N_2$ proposed by Kuafman and Kelso [101], Fishburne and Edse [102], and Mebel et al. [103].

NO converts to NO_2 easily when O_2 is present, even at room temperature. There are several mechanisms to describe the conversion between NO and NO_2, among which $NO + NO + O_2 = NO_2 + NO_2$ has been widely adopted in chemistry models. The rate coefficient of this pathway has been reported in several studies, presented in the form of either $NO + NO + O_2 = NO_2 + NO_2$ [105–107] or $NO_2 + NO_2 = NO + NO + O_2$ [108–110], and the commonly used values are summarized in Table 4. The rate coefficient of $NO_2 + NO_2 = NO + NO + O_2$ in the Glarborg model was adopted from the work of Park et al. [108]. Park et al. [108] first measured the rate coefficient of $NO_2 + NO_2 = NO + NO + O_2$ in a shock tube in the temperature range of 602–954 K. Then, they updated the rate parameters with data obtained by Röhrig et al. [109] in a shock tube at a temperature range of 1388–1460 K. The Konnov model adopted the rate coefficients from their previous work [111], which were evaluated based on the experimental data from Ashmore et al. [105], Zimet [110], and Röhrig et al. [109]. The CRECK modeling group [112] adopted the rate coefficients from Tsang and Herron [113], which were modified from the recommendations of Baulch et al. [114] in order to be compatible with the thermodynamics and the rate expression recommended by Baulch et al. [114] for the reverse reaction. As can be seen from Table 4, these rates differed by a factor of ~3, which could lead to significant uncertainties in predicting NO/NO_2 conversion.

Table 4. The rate coefficients of $NO_2 + NO_2 = NO + NO + O_2$ from different studies.

$NO_2 + NO_2 = NO + NO + O_2$			
	A (cm^3/mole·s)	***n***	**Ea (kcal/mol)**
Glarborg et al. [24]	4.50×10^{12}	0.000	27.599
Konnov et al. [23]	3.95×10^{12}	0.000	27.590
CRECK [112]	1.63×10^{12}	0.000	26.030
Baulch et al. [114]	2.00×10^{12}	0.000	26.825

In addition to the inconsistency in the rate coefficients of $NO_2 + NO_2 = NO + NO + O_2$, there has also been an ongoing controversy regarding the conversion mechanisms between NO and NO_2. The single-step conversion pathway is a trimolecular reaction, which requires three molecules to collide at the same time. This is less likely to happen compared to bimolecular reactions, particularly at low temperatures. As such, mechanisms involving more than one step of bimolecular reactions have also been proposed for conversion between NO and NO_2 [106,115,116]. One of the proposed multi-step conversion mechanisms (referred to as Mech 2 in the following) is

$$NO + O_2 = NO_3 \quad (1)$$

$$NO_3 + NO = NO_2 + NO_2 \quad (2)$$

where the NO reacts with O_2 to form NO_3, then another NO to form two NO_2 molecules.

Another proposed multi-step mechanism (referred to as Mech 3 in the following) is

$$NO + NO = (NO)_2 \quad (3)$$

$$(NO)_2 + O_2 = NO_2 + NO_2 \quad (4)$$

which involves the formation of a dimer from two NO molecules. The dimer further reacts with O_2 to form two NO_2 molecules [117]. Although Mech 2 was included in the Konnov model and the CRECK model, some preliminary kinetic analyses (whose results will be included in a forthcoming publication from the authors' group) have indicated that the NO to NO_2 conversion around room temperature is still dominated by $NO + NO + O_2 = NO_2 + NO_2$. However, other studies have observed experimental trends that might support the dominance of Mech 2 and Mech 3. For instance, Tipper and Williams [107] found that the rate of NO oxidated to NO_2 was about the second order of NO and the first order of O_2 at low temperatures. Both orders decreased when the partial pressure of NO was increased. The authors were able to explain this phenomenon using Mech 2, instead of the single-step conversion mechanism. Solc [118] observed that the NO to NO_2 conversion rate exhibited a strong dependence on the ratio of the initial molar concentrations of O_2 and NO, i.e., $[O_2]/[NO]$. Furthermore, the conversion rate decreased rapidly when $[O_2]/[NO]$ increased from 0 to 10, then decreased gradually until $[O_2]/[NO]$ reached 20 and remained almost constant until $[O_2]/[NO]$ reached 30. This unique trend could not be explained by the single-step conversion mechanism alone, while it could be somewhat explained by Mech 3. The actual mechanisms for NO to NO_2 conversion remain unclear but are expected to be clarified in another forthcoming study from the author's group.

Apart from the conversion pathways reviewed above, $NO + HO_2 = NO_2 + OH$ is another pathway that is important for not only NO and NO_2 conversion but also hydrocarbon and NO_x interaction. This reaction is therefore reviewed briefly below. The contribution of this reaction to the promoting effect of NO on fuel reactivity has been highlighted by many studies [31,33,34], as it is via this reaction that NO converts less reactive HO_2 radicals into more reactive OH radicals. Chakraborty et al. [119] theoretically determined the rate of HO_2 and NO production by $NO_2 + OH$ via the HOONO transition state using high-level ab initio calculations, and the results fit quite well with available experimental data in the form of rate coefficient measurements. Howard [120] measured both the forward and reverse rate coefficients of $NO + HO_2 = NO_2 + OH$ in a flow reactor. After combining this with previously published rate coefficient data for the forward reaction [121] obtained at 232–403 K, a refitted rate coefficient was proposed, which was applicable for the temperature range of 232–1270 K. Badwell et al. [122] determined the rate coefficient of $NO + HO_2 = NO_2 + OH$ and its temperature and pressure dependence and found that the rate coefficient was invariant with pressure.

3.3. Important Direct Interacting Reactions between NO_x and Unsaturated Hydrocarbons

3.3.1. RH + NO_2 Pathways

The dehydrogenation of fuel molecules by oxygen molecules and free radicals plays an important role in fuel oxidation at low temperatures, when it is challenging for unimolecular decomposition to take place. When NO_2 is present, it can act as a free radical and participate in the dehydrogenation of fuel molecules, forming HONO or HNO_2. The importance of H-atom abstraction by NO_2 from fuel molecules has already been highlighted, as it can promote low-temperature OH branching [123] by forming OH and NO via HONO decomposition [89]. The formed NO can further facilitate OH production via $HO_2 + NO = OH + NO_2$ [48]. With unsaturated hydrocarbons, NO_2 can also lose an O atom to the double or triple carbon–carbon bond, producing NO and an aldehyde or an R-oxyl species.

Several works have attempted to determine the rate coefficients for interacting reactions between alkenes/alkynes and NO_2, as summarized in Table 5. Gao et al. [124] obtained the rate coefficients for C_2H_4 and NO_2 interaction reactions using ab initio calculations. Four channels were identified, i.e., $C_2H_4 + NO_2 = CH_3CHO + NO$, $C_2H_4 + NO_2$ = oxirane + NO, $C_2H_4 + NO_2 = C_2H_3 + HONO$, and $C_2H_4 + NO_2 = C_2H_3 + HNO_2$. Chai and Goldsmith [125] adopted density functional theory (DFT) to calculate the rate coefficients for C_3-C_4 alkenes + $NO_2 \rightarrow$ products, including C_3H_6, 1-C_4H_8, trans-2-C_4H_8, and iso-C_4H_8. For each reaction, three types of products were considered, namely cis-HONO, trans-HONO, and HNO_2. The authors found that the interaction was dominated by the channel that formed R and cis-HONO, followed by the channel that formed R and HNO_2. Thomas [126] experimentally measured the rate of C_2H_2 oxidation by NO_2 and determined the respective rate coefficient. However, they were not able to separate different reaction channels. Marshall et al. [54] also calculated the rate coefficient of $C_2H_2 + NO_2$ = CHCHO + NO using transition state theory and found that the rate was pressure-dependent. Sprung et al. [127] experimentally determined the rate coefficients for cis-trans isomerizations of 2-C_4H_8 and 2-C_5H_{10} with NO_2, based on which they estimated the rate coefficients for the addition of NO_2 to the double bond of 10 olefins, i.e., C_2H_2, C_2H_4, C_3H_6, 1-C_4H_8, i-C_4H_8, cis-2-C_4H_8, trans-2-C_4H_8, 1-C_5H_{10}, cis-2-C_5H_{10}, and trans-2-C_5H_{10}, forming adducts, e.g., $C_2H_2NO_2$, $C_2H_4NO_2$, and $C_3H_6NO_2$.

3.3.2. RH + N_2O Pathways

As briefly mentioned in the introduction, the O atom from N_2O tends to be added to the double bond of the unsaturated hydrocarbon. The products depend on the position of the double bond in the unsaturated hydrocarbon. For instance, as shown in Figure 25, if the C=C is located at the terminal of the molecule, the reaction with N_2O can lead to the formation of ketones or aldehydes, depending on which carbon atom the O atom is bonded to [128]. This was first discovered by Bridson-Jones et al. [129,130] in 1951. To date, most studies related to such pathways have been conducted in the liquid phase. For instance, Avdeev et al. [131] determined the reaction pathways for the direct oxidation of cyclohexene and butene with N_2O into carbonyl compounds using DFT. Two possible reaction channels were proposed. Panov et al. [132] and Dubkov et al. [133] studied the oxidation of cyclopentene and cyclohexene with nitrous oxide at high temperatures in the liquid phase. The reaction of the O atom transferring from the N_2O to the C=C bond was found to have a selectivity of nearly 100%. Ivanov et al. [18] used 3-heptene to study the effect of cis/trans isomerism on the reactivity of olefins with N_2O. The experimental results revealed that cis- and trans-isomers of 3-heptene had similar reactivity and yielded the same set of products.

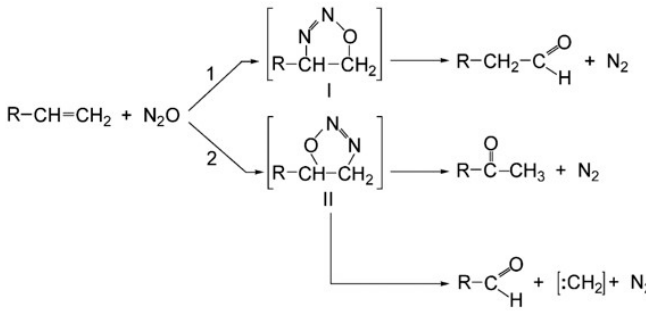

Figure 25. Formation of ketones and aldehydes via direct interacting pathways between N_2O and an unsaturated hydrocarbon with terminal C=C [128].

Table 5. Theoretical and experimental studies on alkene/alkyne +NO_2 reactions and the proposed rate parameters.

Author	Species	Reaction	A (cm^3/mole·s)	*n*	Ea (kcal/mol)
Gao et al. [124]	C_2H_4	$C_2H_4 + NO_2 = CH_3CHO + NO$	4.34×10^{56}	−14.2	51.92
		$C_2H_4 + NO_2 =$ Oxirane + NO	6.62×10^{45}	−11.3	37.81
		$C_2H_4 + NO_2 = C_2H_3 + HONO$	2.13×10^{1}	3.9	30.19
		$C_2H_4 + NO_2 = C_2H_3 + HNO_2$	4.31×10^{0}	3.9	30.19
Chai and Goldsmith [125]	C_3H_6, 1-C_4H_8, trans-2-C_4H_8, iso-C_4H_8	$C_3H_6 + NO_2 = C_3H_5$ + cis-HONO	4.47×10^{-4}	4.79	18.16
		$C_3H_6 + NO_2 = C_3H_5$ + trans-HONO	2.63×10^{-6}	5.32	25.18
		$C_3H_6 + NO_2 = C_3H_5 + HNO_2$	2.54×10^{-2}	4.21	18.76
		1-$C_4H_8 + NO_2$ = 1-C_4H_7 + cis-HONO	3.11×10^{-3}	4.4	15.75
		1-$C_4H_8 + NO_2$ = 1-C_4H_7 + trans-HONO	1.35×10^{-3}	4.47	24.46
		1-$C_4H_8 + NO_2$ = 1-$C_4H_7 + HNO_2$	7.83×10^{-2}	3.93	15.25
		Trans-2-$C_4H_8 + NO_2$ = trans-2-C_4H_7 + cis-HONO	1.31×10^{-3}	4.62	17.36
		Trans-2-$C_4H_8 + NO_2$ = trans-2-C_4H_7 + trans-HONO	1.86×10^{-6}	5.29	22.58
		Trans-2-$C_4H_8 + NO_2$ = trans-2-$C_4H_7 + HNO_2$	4.89×10^{-2}	4.06	17.66
		Iso-2-$C_4H_8 + NO_2$ = iso-2-C_4H_7 + cis-HONO	1.67×10^{-3}	4.56	16.46
		Iso-2-$C_4H_8 + NO_2$ = iso-2-C_4H_7 + trans-HONO	8.91×10^{-6}	5.18	22.98
		Iso-2-$C_4H_8 + NO_2$ = iso-2-C_4H_7+ HNO_2	1.51×10^{-1}	3.95	17.76
Thomas [126]	C_2H_2	$C_2H_2 + NO_2$ = products + NO	1.26×10^{12}		15.05
Marshall et al. [54]	C_2H_2	$C_2H_2 + NO_2 = CHCHO + NO$	1.42×10^{3}	2.79	16.76
Sprung et al. [127]	C_2H_2, C_2H_4, C_3H_6, 1-C_4H_8, i-C_4H_8, cis-2-C_4H_8, trans-2-C_4H_8, 1-C_5H_{10}, cis-2-C_5H_{10}, trans-2-C_5H_{10}	$C_2H_2 + NO_2$ = adduct	5.83×10^{12}	-	14.40
		$C_2H_4 + NO_2$ = adduct	9.33×10^{12}	-	14.00
		$C_3H_6 + NO_2$ = adduct	2.48×10^{12}	-	27.10
		1-$C_4H_8 + NO_2$ = adduct	1.82×10^{12}	-	25.00
		I-$C_4H_8 + NO_2$ = adduct	4.37×10^{12}	-	28.70
		Cis-2-$C_4H_8 + NO_2$ = adduct	4.41×10^{11}	-	11.40
		Trans-2-$C_4H_8 + NO_2$ = adduct	7.47×10^{11}	-	11.60
		1-$C_5H_{10} + NO_2$ = adduct	1.70×10^{12}	-	24.70
		Cis-2-$C_5H_{10} + NO_2$ = adduct	4.81×10^{11}	-	23.20
		Trans-2-$C_5H_{10} + NO_2$ = adduct	9.70×10^{11}	-	23.40

In the gas phase, only a few studies have focused on this pathway, which are listed in Table 6. Due to the lack of relevant studies, this pathway is absent from almost all existing chemistry models. Nevertheless, it can be quite common for such interactions to occur between unsaturated hydrocarbons and N_2O, especially at low to moderate temperatures, which are relevant for combustion applications. Trenwith [64] experimentally recorded the partial pressure of reactants (i.e., C_2H_4 and N_2O) and products (e.g., N_2, CO, CH_4, H_2, and C_2H_4O) and determined the rate coefficient of $C_2H_4 + N_2O = CH_3CHO + N_2$ at 828–863 K. Karami and Vahedpour [134] investigated the reaction pathway of $C_2H_2 + N_2O$ → products using high-level ab initio calculations. The results revealed that $CH_2CO + N_2$ was the most favored adduct of $C_2H_2 + N_2O$. Furthermore, several studies have tried to investigate the 1,3-dipolar cycloadditions of unsaturated hydrocarbons and N_2O. Ess and Houk [135] evaluated the activation barriers and reaction energetics for cycloaddition reactions of C_2H_4 and C_2H_2 by N_2O using DFT, MP2, and CBS-QB3 methods. Grimme et al. [136] also studied the cycloaddition reactions of dipolar molecules to C_2H_4 and C_2H_2. N_2O was one of the investigated dipolar molecules. The reaction potential energy surfaces of $C_2H_2 + N_2O = (CH)_2ON_2$ and $C_2H_4 + N_2O = (CH_2)_2ON_2$ were obtained by quantum

chemical methods. Liu and Li [137] determined the accurate full-dimensional potential energy surface of the C_2H_2 + N_2O = oxadiazole reaction in the gas phase, which was fitted to about 64,000 high-level ab initio data using a machine learning approach. Li et al. [138] calculated the reaction pathway of C_2H_4 + N_2O → products using DFT methods. The results indicated that the reaction preferred the mechanism that included the addition of N_2O to the double bond of C_2H_4.

Table 6. Theoretical and experimental studies on C_2-alkene/alkyne +N_2O reactions and the proposed rate parameters.

Author	Species	Reaction	A (cm^3/mole·s)	*n*	Ea (kcal/mole)
Trenwith [64]	C_2H_4	$C_2H_4 + N_2O = C_2H_4O + N_2$	7.95×10^9	-	38.13
Karami and Vahedpour [134] *	C_2H_2	$C_2H_2 + N_2O = CH_2CO + N_2$	-	-	-
Ess and Houk [135] *	C_2H_2	$C_2H_2 + N_2O = (CH)_2ON_2$	-	-	-
	C_2H_4	$C_2H_4 + N_2O = (CH_2)_2ON_2$	-	-	-
Grimme et al. [136] *	C_2H_2	$C_2H_2 + N_2O = (CH)_2ON_2$	-	-	-
	C_2H_4	$C_2H_4 + N_2O = (CH_2)_2ON_2$	-	-	-
Liu and Li [137] *	C_2H_2	$C_2H_2 + N_2O = (CH)_2ON_2$	-	-	-
Li et al. [138] *	C_2H_4	$C_2H_4 + N_2O = (CH_2)_2ON_2$	-	-	-

* *ab initio* calculations without providing proposed rate parameters.

3.3.3. ROO + NO

After the dehydrogenation of RH, O_2 is added to R radicals to form ROO. NO can abstract an O atom from ROO radicals to form RO and NO_2 or bond with ROO to form $RONO_2$. These two reaction channels are also important interactions between unsaturated hydrocarbons and NO_x during combustion. Many works have already emphasized the importance of ROO + NO reactions for saturated hydrocarbons mixed with NO_x [48]. Atkinson et al. [139] reviewed the studies on CH_3O_2 + NO = CH_3O + NO_2 from 1981 to 2004 and proposed the rate coefficient of this reaction at 200–430 K. Maricq and Szente [140] experimentally determined the rate coefficient of $C_2H_5O_2$ + NO = C_2H_5O + NO_2 using transient diode laser absorption and time-resolved UV spectroscopy. Chow et al. [141] determined the total rate coefficient for $C_3H_7O_2$ + NO → products and for the minor branching channel, which forms i-$C_3H_7ONO_2$ as a product, at temperatures of 298–213 K using a turbulent flow tube. The rate coefficients of larger alkyl peroxides, e.g., $C_4H_9O_2$ and $C_8H_{17}O_2$, reacting with NO are also available in the literature [142–144].

However, studies on the rate coefficient of ROO + NO → products, with ROO derived from unsaturated hydrocarbons, are scarce, as summarized in Table 7. Eberhard and Howard [145] determined the rate coefficient of $C_3H_5O_2$ (CH_2 = $CHCH_2OO$) + NO in a flow tube reactor at 297 K. Feng et al. [146] studied the potential energy surface of benzyl peroxy radicals reacting with NO using ab initio calculations, considering channels leading to the production of $C_6H_5CH_2O$ and NO_2, and $C_6H_5CH_2ONO_2$.

Table 7. Theoretical and experimental studies on ROO + NO reactions and their proposed rate parameters.

Author	Species	Reaction	A (cm^3/mole·s)	*n*	Ea (kcal/mole)
Eberhard and Howard [145]	$C_3H_5O_2$	$C_3H_5O_2$ + NO = product	6.32×10^{12}	-	-
Feng et al. [146] *	$C_6H_5CH_2O_2$	$C_6H_5CH_2O_2$ + NO = $C_6H_5CH_2O$+ NO_2	-	-	-
		$C_6H_5CH_2O_2$ + NO = $C_6H_5CH_2ONO_2$	-	-	-

* *ab initio* calculations without providing proposed rate parameters.

4. Conclusions and Recommendations

This paper presented a comprehensive review on the combustion chemistry of unsaturated/oxygenated hydrocarbons mixed with NO_x species (namely NO, NO_2, and N_2O). The literature published since the early 1950s was surveyed to provide a comprehensive summary of experimental and theoretical studies. Through these studies, NO_x blending effects were analyzed using fundamental combustion experiments (i.e., IDT, LBV, and speciation) obtained from RCMs, shock tubes, flame burners, flow reactors, and JSRs; the underlying chemistries, particularly the unsaturated hydrocarbon/NO_x interaction chemistry and the NO_x conversion chemistry, were highlighted using direct experiments for reaction rate measurements, ab initio calculations, and chemical kinetic modeling. The knowledge compiled in this study has enabled a better understanding of the combustion features for this type of mixture and the governing chemistry, which is beneficial for future applications in practical engines and the development of robust chemical kinetic models.

The key insights and prospects for future experimental and theoretical studies are summarized as follows:

1. There is an immense need for fundamental combustion experiments, with a special emphasis on NO_2 and N_2O; heavier unsaturated hydrocarbons (i.e., carbon number > 3); and high-pressure conditions (e.g., >40 bar). It is still obvious based on the limited data that the effects of NO_x blending on the reactivity of unsaturated hydrocarbons are diverse. In general, NO and NO_2 promote fuel reactivity at low temperatures. This promoting effect diminishes as the temperature increases and can even be reversed at high temperatures, when NO and NO_2 start to inhibit fuel reactivity. The blending effects of N_2O are less clear, as it has mostly been used directly as an oxidizer, quickly decomposing to produce O atoms via $N_2O(+M) = N_2 + O(+M)$. As such, fundamental combustion experiments over wider ranges of conditions are highly recommended to re-evaluate the effects of NO_x blending on unsaturated hydrocarbon combustion characteristics in a consistent manner, and to distinguish the effects of NO_x blending between unsaturated and saturated hydrocarbons.
2. The diverse effects of NO_x blending are further complicated by the interconversion between the NO_x species, for which the available conversion mechanisms remain controversial. This is most prominent for the conversion between NO and NO_2, which has been observed to exhibit both second and third reaction orders and both strong and weak dependence on the O_2 concentration. Experimental and theoretical studies on NO_x interconversions are urgently needed to account for their impact on the effects of NO_x blending, as well as to guide future fundamental combustion experiments in properly preparing fuel/NO_x/oxidizer mixtures.
3. There is a unique interaction between NO_x and unsaturated hydrocarbons, with NO_2 and N_2O able to bond directly to the carbon–carbon double and triple bonds. These interacting pathways depend highly on pressure (due to the imbalance in molar number across the reaction), which might substantially alter the effects of NO_x blending under the high-pressure conditions that are relevant to advanced combustion engines. In addition, other types of direct interaction, such as $RH + NO_2 = R + HONO$ (or HNO_2) and $ROO + NO = RO + NO_2$, have also been highlighted as holding significance. Currently, the understanding of these interactions is seriously lacking, let alone their impact on the effects of NO_x blending. Further investigations into these interactions are therefore highly recommended. In addition to fundamental experiments, theoretical studies such as ab initio calculations could be quite valuable to determine the specific reaction channels involved in these interactions and establish the respective rate rules.
4. The existing chemical kinetic models are inadequate and inconsistent in replicating the combustion characteristics of unsaturated hydrocarbon/NO_x mixtures. To date, the pathways of NO_2 and N_2O bonding to unsaturated carbon–carbon bonds have been rarely addressed, and NO_x interconversions are insufficiently represented in existing chemical kinetic models. The situation has been made worse by the limitations of

available fundamental combustion experiments and theoretical studies. Systematic efforts, such as those pointed out in (1)–(3), are necessary to address the inconsistencies and inadequacies of existing models for unsaturated hydrocarbon/NO_x mixtures.

Author Contributions: Conceptualization, R.T. and S.C.; methodology, R.T. and S.C.; software, R.T. and S.C.; validation, R.T. and S.C.; formal analysis, R.T. and S.C.; investigation, R.T. and S.C.; resources, R.T. and S.C.; data curation, R.T. and S.C.; writing—original draft preparation, R.T. and S.C.; writing—review and editing, S.C.; visualization, S.C.; supervision, S.C.; project administration, S.C.; funding acquisition, S.C. All authors have read and agreed to the published version of the manuscript.

Funding: This work was supported by the Research Grants Council of the Hong Kong Special Administrative Region, China, under grants PolyU P0034937 and PolyU P0039589.

Data Availability Statement: Not applicable.

Conflicts of Interest: The authors declare no conflict of interest.

References

1. Pu, W.; Sun, D.; Fan, W.; Pan, W.; Chai, Q.; Wang, X.; Lv, Y. Cu-Catalyzed atom transfer radical addition reactions of alkenes with alpha-bromoacetonitrile. *Chem. Commun.* **2019**, *55*, 4821–4824. [CrossRef] [PubMed]
2. Zamir, E.; Haas, Y.; Levine, R.D. Laser enhanced addition reactions between hydrogen halides and unsaturated hydrocarbons: An information–theoretic approach. *J. Chem. Phys.* **1980**, *73*, 2680–2687. [CrossRef]
3. Preston, T.J.; Dunning, G.T.; Orr-Ewing, A.J.; Vazquez, S.A. Direct and indirect hydrogen abstraction in Cl + alkene reactions. *J. Phys. Chem. A* **2014**, *118*, 5595–5607. [CrossRef] [PubMed]
4. Mehl, M.; Pitz, W.J.; Westbrook, C.K.; Yasunaga, K.; Conroy, C.; Curran, H.J. Autoignition behavior of unsaturated hydrocarbons in the low and high temperature regions. *Proc. Combust. Inst.* **2011**, *33*, 201–208. [CrossRef]
5. Seleznev, R.K.; Surzhikov, S.T.; Shang, J.S. A review of the scramjet experimental data base. *Prog. Aerosp. Sci.* **2019**, *106*, 43–70. [CrossRef]
6. Zhou, C.W.; Farooq, A.; Yang, L.; Mebel, A.M. Combustion chemistry of alkenes and alkadienes. *Prog. Energy Combust. Sci.* **2022**, *90*, 100983. [CrossRef]
7. Garner, S.; Sivaramakrishnan, R.; Brezinsky, K. The high-pressure pyrolysis of saturated and unsaturated C7 hydrocarbons. *Proc. Combust. Inst.* **2009**, *32*, 461–467. [CrossRef]
8. Wolk, B.; Ekoto, I.; Northrop, W.F.; Moshammer, K.; Hansen, N. Detailed speciation and reactivity characterization of fuel-specific in-cylinder reforming products and the associated impact on engine performance. *Fuel* **2016**, *185*, 348–361. [CrossRef]
9. Pool-Zobel, B.L.; Schmezer, P.; Zeller, W.J.; Klein, R.G. In vitro and ex vivo effects of the air pollutants SO_2 and NO_x on benzo(a)pyrene activating enzymes of the rat liver. *Exp. Pathol.* **1990**, *39*, 207–212. [CrossRef]
10. Kramlich, J.C.; Linak, W.P. Nitrous oxide behavior in the atmosphere, and in combustion and industrial systems. *Prog. Energy Combust. Sci.* **1994**, *20*, 149–202. [CrossRef]
11. Hill, S.C.; Douglas Smoot, L. Modeling of nitrogen oxides formation and destruction in combustion systems. *Prog. Energy Combust. Sci.* **2000**, *26*, 417–458. [CrossRef]
12. Razus, D. Nitrous Oxide: Oxidizer and Promoter of Hydrogen and Hydrocarbon Combustion. *Ind. Eng. Chem. Res.* **2022**, *61*, 11329–11346. [CrossRef]
13. Zakirov, V.; Sweeting, M.; Lawrence, T.; Sellers, J. Nitrous oxide as a rocket propellant. *Acta Astronaut.* **2001**, *48*, 353–362. [CrossRef]
14. Sahu, A.B.; Mohamed, A.A.E.-S.; Panigrahy, S.; Saggese, C.; Patel, V.; Bourque, G.; Pitz, W.J.; Curran, H.J. An experimental and kinetic modeling study of NO_x sensitization on methane autoignition and oxidation. *Combust. Flame* **2022**, *238*, 111746. [CrossRef]
15. Zhai, Y.; Xu, Q.; Feng, B.; Shao, C.; Wang, Z.; Sarathy, S.M. Impacts of NO on low-temperature oxidation of n-heptane in a jet-stirred reactor. *Combust. Flame* **2023**, *253*, 112824. [CrossRef]
16. Yu, B.; Kum, S.-M.; Lee, C.-E.; Lee, S. Study on the combustion characteristics of a premixed combustion system with exhaust gas recirculation. *Energy* **2013**, *61*, 345–353. [CrossRef]
17. Mahla, S.K.; Dhir, A.; Gill, K.J.S.; Cho, H.M.; Lim, H.C.; Chauhan, B.S. Influence of EGR on the simultaneous reduction of NO_x-smoke emissions trade-off under CNG-biodiesel dual fuel engine. *Energy* **2018**, *152*, 303–312. [CrossRef]
18. Ivanov, D.; Babushkin, D.; Semikolenov, S.; Malykhin, S.; Kharitonov, A.; Dubkov, K. Effect of cis/trans isomerism on selective oxidation of olefins with nitrous oxide. *Tetrahedron* **2016**, *72*, 2501–2506. [CrossRef]
19. Starokon, E.V.; Dubkov, K.A.; Babushkin, D.E.; Parmon, V.N.; Panov, G.I. Liquid Phase Oxidation of Alkenes with Nitrous Oxide to Carbonyl Compounds. *Adv. Synth. Catal.* **2004**, *346*, 268–274. [CrossRef]
20. Semikolenov, S.V.; Dubkov, K.A.; Starokon, E.V.; Babushkin, D.E.; Panov, G.I. Liquid-phase noncatalytic butene oxidation with nitrous oxide. *Russ. Chem. Bull.* **2005**, *54*, 948–956. [CrossRef]

21. Konnov, A.A. Detailed Reaction Mechanism for Small Hydrocarbons Combustion, Release 0.5. 2000. Available online: https://homepages.vub.ac.be/~akonnov/ (accessed on 23 May 2023).
22. Coppens, F.; Deruyck, J.; Konnov, A. The effects of composition on burning velocity and nitric oxide formation in laminar premixed flames of $CH_4 + H_2 + O_2 + N_2$. *Combust. Flame* **2007**, *149*, 409–417. [CrossRef]
23. Konnov, A.A. Implementation of the NCN pathway of prompt-NO formation in the detailed reaction mechanism. *Combust. Flame* **2009**, *156*, 2093–2105. [CrossRef]
24. Glarborg, P.; Miller, J.A.; Ruscic, B.; Klippenstein, S.J. Modeling nitrogen chemistry in combustion. *Prog. Energy Combust. Sci.* **2018**, *67*, 31–68. [CrossRef]
25. Wu, Y.; Panigrahy, S.; Sahu, A.B.; Bariki, C.; Liang, J.; Mohamed, A.; Dong, S.; Tang, C.; Pitsch, H.; Huang, Z.; et al. Understanding the antagonistic effect of methanol as a component in surrogate fuel models: A case study of methanol/n-heptane mixtures. *Combust. Flame* **2021**, *226*, 229–242. [CrossRef]
26. Doughty, A.; Barnes, F.J.; Bromly, J.H.; Haynes, B.S. The mutually sensitied oxidation of ethylene and NO: An experimental and kinetic modeling study. *Symp. Int. Combust.* **1996**, *26*, 589–596. [CrossRef]
27. Dagaut, P.; Lecomte, F.; Chevailler, S.; Cathonnet, M. The reduction of NO by ethylene in a jet-stirred reactor at 1 atm: Experimental and kinetic modelling. *Combust. Flame* **1999**, *119*, 494–504. [CrossRef]
28. Dagaut, P.; Mathieu, O.; Nicolle, A.; Dayma, G. Experimental Study and Detailed Kinetic Modeling of the Mutual Sensitization of the Oxidation of Nitric Oxide, Ethylene, and Ethane. *Combust. Sci. Technol.* **2005**, *177*, 1767–1791. [CrossRef]
29. Giménez-López, J.; Alzueta, M.U.; Rasmussen, C.T.; Marshall, P.; Glarborg, P. High pressure oxidation of C_2H_4/NO mixtures. *Proc. Combust. Inst.* **2011**, *33*, 449–457. [CrossRef]
30. Atakan, B.; Hartlieb, A.T. Laser diagnostics of NO reburning in fuel-rich propene flames. *Appl. Phys. B* **2014**, *71*, 697–702. [CrossRef]
31. Dagaut, P.; Luche, J.; Cathonnet, M. Experimental and kinetic modeling of the reduction of NO by propene at 1 atm. *Combust. Flame* **2000**, *121*, 651–661. [CrossRef]
32. Yuan, W.; Ruwe, L.; Schwarz, S.; Cao, C.; Yang, J.; Deutschmann, O.; Kohse-Höinghaus, K.; Qi, F. Insights into the interaction kinetics between propene and NO_x at moderate temperatures with experimental and modeling methods. *Proc. Combust. Inst.* **2021**, *38*, 795–803. [CrossRef]
33. Gossler, S.; Ruwe, L.; Yuan, W.; Yang, J.; Chen, X.; Schmitt, S.; Maier, L.; Kohse-Höinghaus, K.; Qi, F.; Deutschmann, O. Exploring the interaction kinetics of butene isomers and NO_x at low temperatures and diluted conditions. *Combust. Flame* **2021**, *233*, 111557. [CrossRef]
34. Prabhu, S.K.; Bhat, R.K.; Miller, D.L.; Cernansky, N.P. 1-Pentene oxidation and its interaction with nitric oxide in the low and negative temperature coefficient regions. *Combust. Flame* **1996**, *104*, 377–390. [CrossRef]
35. Quang, L.N.; Vanpee, M. A spectroscopic investigation of the premixed acetylene-nitric oxide flame. *Symp. Int. Combust.* **1982**, *19*, 293–301. [CrossRef]
36. Quang Ngoc, L.; Vanpee, M. Free radical concentration measurements in nitric oxide acetylene flames. *Combust. Flame* **1985**, *62*, 193–210. [CrossRef]
37. Dagaut, P.; Lecomte, F.; Chevailler, S.; Cathonnet, M. Experimental and kinetic modeling of nitric oxide reduction by acetylene in an atmospheric pressure jet-stirred reactor. *Fuel* **1999**, *78*, 1245–1252. [CrossRef]
38. Guarneri, F.; Ikeda, E.; Mackie, J.C. A Study of Furan as a Model Oxygenated Reburn Fuel for Nitric Oxide Reduction. *Energ Fuels* **2001**, *2001*, 743–750. [CrossRef]
39. Alexandrino, K.; Millera, Á.; Bilbao, R.; Alzueta, M.U. Interaction between 2,5-Dimethylfuran and Nitric Oxide: Experimental and Modeling Study. *Energy Fuels* **2014**, *28*, 4193–4198. [CrossRef]
40. Alexandrino, K.; Millera, Á.; Bilbao, R.; Alzueta, M.U. 2-methylfuran Oxidation in the Absence and Presence of NO. *Flow Flow Turbul. Combust. Flow* **2015**, *96*, 343–362. [CrossRef]
41. Alzueta, M.U.; Serinyel, Z.; Simmie, J.M.; Curran, H.J. Oxidation of Acetone and Its Interaction with Nitric Oxide. *Energy Fuels* **2010**, *24*, 1511–1520. [CrossRef]
42. Williams, B.A.; Pasternack, L. The effect of nitric oxide on premixed flames of CH_4, C_2H_6, C_2H_4, and C_2H_2. *Combust. Flame* **1997**, *111*, 87–110. [CrossRef]
43. Glarborg, P.; Alzueta, M.U.; Dam-Johansen, K.; Miller, J.A. Kinetic Modeling of Hydrocarbon/Nitric Oxide Interactions in a Flow Reactor. *Combust. Flame* **1998**, *115*, 1–27. [CrossRef]
44. Konnov, A.A.; Dyakov, I.V.; Knyazkov, D.A.; Korobeinichev, O.P. Formation and Destruction of Nitric Oxide in NO Doped Premixed Flames of C_2H_4, C_2H_6, and C_3H_8 at Atmospheric Pressure. *Energy Fuels* **2010**, *24*, 4833–4840. [CrossRef]
45. Hori, M.; Matsunaga, N.; Marinov, N.; William, P.; Charles, W. An experimental and kinetic calculation of the promotion effect of hydrocarbons on the NO-NO_2 conversion in a flow reactor. *Symp. Int. Combust.* **1998**, *27*, 389–396. [CrossRef]
46. Abián, M.; Silva, S.L.; Millera, Á.; Bilbao, R.; Alzueta, M.U. Effect of operating conditions on NO reduction by acetylene–ethanol mixtures. *Fuel Process. Technol.* **2010**, *91*, 1204–1211. [CrossRef]
47. Marrodán, L.; Berdusán, L.; Aranda, V.; Millera, Á.; Bilbao, R.; Alzueta, M.U. Influence of dimethyl ether addition on the oxidation of acetylene in the absence and presence of NO. *Fuel* **2016**, *183*, 1–8. [CrossRef]
48. Cheng, S.; Saggese, C.; Goldsborough, S.S.; Wagnon, S.W.; Pitz, W.J. Unraveling the role of EGR olefins at advanced combustion conditions in the presence of nitric oxide: Ethylene, propene and isobutene. *Combust. Flame* **2022**, *245*, 112344. [CrossRef]

49. Alzueta, M.U.; Glarborg, P.; Dam-Johansen, K. Low temperature interactions between hydrocarbons and nitric oxide: An experimental study. *Combust. Flame* **1997**, *109*, 25–36. [CrossRef]
50. Abián, M.; Peribáñez, E.; Millera, Á.; Bilbao, R.; Alzueta, M.U. Impact of nitrogen oxides (NO, NO_2, N_2O) on the formation of soot. Combust. *Flame* **2014**, *161*, 280–287. [CrossRef]
51. Menon, A.V.; Lee, S.-Y.; Linevsky, M.J.; Litzinger, T.A.; Santoro, R.J. Addition of NO_2 to a laminar premixed ethylene–air flame: Effect on soot formation. *Proc. Combust. Inst.* **2007**, *31*, 593–601. [CrossRef]
52. Deng, F.; Zhang, Y.; Sun, W.; Huang, W.; Zhao, Q.; Qin, X.; Yang, F.; Huang, Z. Towards a kinetic understanding of the NO_x sensitization effect on unsaturation hydrocarbons: A case study of ethylene/nitrogen dioxide mixtures. *Proc. Combust. Inst.* **2019**, *37*, 719–726. [CrossRef]
53. Volponi, J.V.; Branch, M.C. Flame structure of C_2H_2-O_2-Argon and C_2H_2-NO_2- Argon laminar premixed flames. *Symp. Int. Combust.* **1992**, *24*, 823–831. [CrossRef]
54. Marshall, P.; Leung, C.; Gimenez-Lopez, J.; Rasmussen, C.T.; Hashemi, H.; Glarborg, P.; Abian, M.; Alzueta, M.U. The C_2H_2 + NO_2 reaction: Implications for high pressure oxidation of C_2H_2/NO_x mixtures. *Proc. Combust. Inst.* **2019**, *37*, 469–476. [CrossRef]
55. Jin, Y.; Ma, Z.; Wang, X.; Liu, F.; Li, X.; Chu, X. Experimental and Kinetic Study of the Effect of Nitrogen Dioxide on Ethanol Autoignition. *ACS Omega* **2023**, *8*, 8377–8387. [CrossRef]
56. Ye, W.; Shi, J.C.; Zhang, R.T.; Wu, X.J.; Zhang, X.; Qi, M.L.; Luo, S.N. Experimental and Kinetic Modeling Study of CH_3OCH_3 Ignition Sensitized by NO_2. *Energy Fuels* **2016**, *30*, 10900–10908. [CrossRef]
57. Alzueta, M.U.; Muro, J.; Bilbao, R.; Glarborg, P. Oxidation of Dimethyl Ether and its Interaction with Nitrogen Oxides. *Isr. J. Chem.* **1999**, *39*, 73–86. [CrossRef]
58. Atkinson, R.; Aschmann, S.M.; Winer, A.M.; Pitts, J.N., Jr. Gas phase reaction of NO_2 with alkenes and dialkenes. *Int. J. Chem. Kinet.* **1984**, *16*, 697–706. [CrossRef]
59. Bernard, F.; Cazaunau, M.; Mu, Y.; Wang, X.; Daele, V.; Chen, J.; Mellouki, A. Reaction of NO_2 with selected conjugated alkenes. *J. Phys. Chem. A* **2013**, *117*, 14132–14140. [CrossRef]
60. Ohta, T.; Nagura, H.; Suzuki, S. Rate constants for the reactions of conjugated olefins with NO_2 in the gas phase. *Int. J. Chem. Kinet.* **1986**, *18*, 1–11. [CrossRef]
61. Harrison, R.M.; Shi, J.P.; Grenfell, J.L. Novel nighttime free radical chemistry in severe nitrogen dioxide pollution episodes. *Atmos. Environ.* **1998**, *32*, 2769–2774. [CrossRef]
62. Shi, J.P.; Harrison, R.M. Rapid NO2 formation in diluted petrol-fuelled engine exhaust—A source of NO_2 in winter smog episodes. *Atmos. Environ.* **1997**, *31*, 3857–3866. [CrossRef]
63. Trenwith, A.B. The kinetics of the oxidation of ethylene by nitrous oxide. *J. Chem. Soc.* **1960**, *743*, 3722–3726. [CrossRef]
64. Howard, S.L.; Newberry, J.E.; Sausa, R.C.; Miziolek, A.W. Triple quadrupole mass spectrometry as applied to flame diagnostics: Study of the C_2H_4/N_2O/Ar Flame. *J. Am. Soc. Mass Spectrom.* **1993**, *4*, 152–158. [CrossRef] [PubMed]
65. Werlin, L.; Felix, L.; Dominic, F.; Nicole, R.; Helmut, C.; Stefan, S. Experimental Investigation of the Flame Propagation and Flashback Behavior of a Green Propellant Consisting of N_2O and C_2H_4. *J. Energy Power Eng.* **2017**, *11*, 735–752.
66. Naumann, C.; Kick, T.; Methling, T.; Braun-Unkhoff, M.; Riedel, U. Ethene/Dinitrogen Oxide—A Green Propellant to substitute Hydrazine: Investigation on its Ignition Delay Time and Laminar Flame Speed. In Proceedings of the 26th ICDERS, Boston, MA, USA, 30 July–4 August 2017.
67. Kick, T.; Starcke, J.H.; Naumann, C. Green Propellant Substituting Hydrazine: Investigation of Ignition Delay Time and Laminar Flame Speed of Ethene/Dinitrogen Oxide Mixtures. In Proceedings of the European Combustion Meeting, Dubrovnik, Croatia, 18–21 April 2017.
68. Deng, F.; Pan, Y.; Sun, W. Comparative Study of the Effects of Nitrous Oxide and Oxygen on Ethylene Ignition. *Energ Fuels* **2017**, *31*, 14116–14128. [CrossRef]
69. Zhang, F.; Chen, H.Y.; Feng, J.C.; Zheng, D. Experimental investigation of auto-ignition of ethylene-nitrous oxide propellants in rapid compression machine. *Fuel* **2021**, *288*, 119688. [CrossRef]
70. Yang, M.; Yang, Y.; Liao, C.; Tang, C.; Zhou, C.-W.; Huang, Z. The auto-ignition boundary of ethylene/nitrous oxide as a promising monopropellant. *Combust. Flame* **2020**, *221*, 64–73. [CrossRef]
71. Wang, W.; Zhang, H. Laminar burning velocities of C_2H_4/N_2O flames: Experimental study and its chemical kinetics mechanism. *Combust. Flame* **2019**, *202*, 362–375. [CrossRef]
72. Aldous, K.M.; Bailey, B.W.; Rankin, J.M. Burning velocity of the premixed nitrous-oxide/acetylene flame and its influence on burner design. *Anal. Chem.* **1972**, *44*, 191–194. [CrossRef]
73. Alekseev, V.A.; Bystrov, N.; Emelianov, A.; Eremin, A.; Yatsenko, P.; Konnov, A.A. High-temperature oxidation of acetylene by N2O at high Ar dilution conditions and in laminar premixed C_2H_2 + O_2 + N_2 flames. *Combust. Flame* **2022**, *238*, 111924. [CrossRef]
74. Powell, O.A.; Papas, P.; Dreyer, C. Laminar Burning Velocities for Hydrogen-, Methane-, Acetylene-, and Propane-Nitrous Oxide Flames. *Combust. Sci. Technol.* **2009**, *181*, 917–936. [CrossRef]
75. Powell, O.A.; Papas, P. Flame Structure Measurements of Nitric Oxide in Hydrocarbon-Nitrous-Oxide Flames. *J. Propul. Power* **2012**, *28*, 1052–1059. [CrossRef]
76. Mével, R.; Shepherd, J.E. Ignition delay-time behind reflected shock waves of small hydrocarbons–nitrous oxide(–oxygen) mixtures. *Shock Waves* **2014**, *25*, 217–229. [CrossRef]

77. Naumann, C.; Kick, T.; Methling, T.; Braun-Unkhoff, M.; Riedel, U. Ethene/Nitrous Oxide Mixtures as Green Propellant to Substitute Hydrazine: Reaction Mechanism Validation. *Int. J. Energ. Mater. Chem. Propul.* **2020**, *19*, 65–71. [CrossRef]
78. Tsang, W. Chemical Kinetic Data Base for Propellant Combustion. II. Reactions Involving CN, NCO, and HNCO. *J. Phys. Chem. Ref. Data* **1992**, *21*, 753–791. [CrossRef]
79. Williams, B.A.; Papas, P.; Nelson, H.H. Kinetics and product channels of the reaction CN + N_2O. *J. Phys. Chem.* **1995**, *99*, 13471–13475. [CrossRef]
80. Xu, S.; Lin, M.C. Ab initio chemical kinetics for the reactions of HNCN with O(3P) and O_2. *Proc. Combust. Inst.* **2009**, *32*, 99–106. [CrossRef]
81. Xu, S.; Lin, M.C. Ab Initio Chemical Kinetics for the OH + HNCN Reaction. *J. Phys. Chem. A* **2007**, *111*, 6730–6740. [CrossRef]
82. Hashemi, H.; Christensen, J.M.; Gersen, S.; Levinsky, H.; Klippenstein, S.J.; Glarborg, P. High-pressure oxidation of methane. *Combust. Flame* **2016**, *172*, 349–364. [CrossRef]
83. Gimenez-Lopez, J.; Rasmussen, C.T.; Hashemi, H.; Alzueta, M.U.; Gao, Y.; Marshall, P.; Goldsmith, C.F.; Glarborg, P. Experimental and Kinetic Modeling Study of C_2H_2 Oxidation at High Pressure. *Int. J. Chem. Kinet.* **2016**, *48*, 724–738. [CrossRef]
84. Hashemi, H.; Jacobsen, J.G.; Rasmussen, C.T.; Christensen, J.M.; Glarborg, P.; Gersen, S.; van Essen, M.; Levinsky, H.B.; Klippenstein, S.J. High-pressure oxidation of ethane. *Combust. Flame* **2017**, *182*, 150–166. [CrossRef]
85. Klippenstein, S.J.; Harding, L.B.; Glarborg, P.; Miller, J.A. The role of NNH in NO formation and control. *Combust. Flame* **2011**, *158*, 774–789. [CrossRef]
86. Dagaut, P.; Glarborg, P.; Alzueta, M. The oxidation of hydrogen cyanide and related chemistry. *Prog. Energy Combust. Sci.* **2008**, *34*, 1–46. [CrossRef]
87. Mendiara, T.; Glarborg, P. Ammonia chemistry in oxy-fuel combustion of methane. *Combust. Flame* **2009**, *156*, 1937–1949. [CrossRef]
88. Mendiara, T.; Glarborg, P. Reburn Chemistry in Oxy-fuel Combustion of Methane. *Energy Fuels* **2009**, *23*, 3565–3572. [CrossRef]
89. Zhou, C.W.; Li, Y.; Burke, U.; Banyon, C.; Somers, K.P.; Ding, S.; Khan, S.; Hargis, J.W.; Sikes, T.; Mathieu, O.; et al. An experimental and chemical kinetic modeling study of 1,3-butadiene combustion: Ignition delay time and laminar flame speed measurements. *Combust. Flame* **2018**, *197*, 423–438. [CrossRef]
90. Yang, C.; Wang, W.; Li, Y.; Cheng, X. Experimental and kinetic study of NO/NO_2 chemical effects on n-heptane high temperature auto-ignition. *Combust. Flame* **2023**, *249*, 112604. [CrossRef]
91. Kaufman, F.; Gerri, N.J.; Bowman, R.E. Role of Nitric Oxide in the Thermal Decomposition of Nitrous Oxide. *J. Chem. Phys.* **1956**, *25*, 106–115. [CrossRef]
92. Baber, S.C.; Dean, A.M. N_2O Dissociation behind reflected shock waves. *Int. J. Chem. Kinet.* **1975**, *7*, 381–398. [CrossRef]
93. Buczkó, N.A.; Varga, T.; Zsély, I.G.; Turányi, T. Formation of NO in High-Temperature $N_2/O_2/H_2O$ Mixtures: Re-evaluation of Rate Coefficients. *Energy Fuels* **2018**, *32*, 10114–10120. [CrossRef]
94. Baldwin, R.R.; Gethin, A.; Plaistowe, J.; Walker, R.W. Reaction between hydrogen and nitrous oxide. *J. Chem. Soc., J. Chem. Soc. Faraday Trans. 1* **1975**, *71*, 1265–1284. [CrossRef]
95. Marshall, P.; Fontijn, A.; Melius, C.F. High-temperature photochemistry and BAC-MP4 studies of the reaction between ground-state H atoms and N_2O. *J. Chem. Phys.* **1987**, *86*, 5540–5549. [CrossRef]
96. Bozzelli, J.W.; Chang, A.Y.; Dean, A.M. Analysis of the reactions H + N_2O and NH + NO: Pathways and rate constants over a wide range of temperature and pressure. *Symp. Int. Combust.* **1994**, *25*, 965–974. [CrossRef]
97. Roose, T.R.; Hanson, R.K.; Kruger, C.H. A shock tube study of the decomposition of no in the presence of NH_3. *Symp. Int. Combust.* **1981**, *18*, 853–862. [CrossRef]
98. Kovács, M.; Papp, M.; Zsély, I.G.; Turányi, T. Determination of rate parameters of key N/H/O elementary reactions based on $H_2/O_2/NO_x$ combustion experiments. *Fuel* **2020**, *264*, 116720. [CrossRef]
99. Park, J.; Hershberger, J.F. A diode laser study of the isocyanate + nitrogen dioxide reaction. *J. Phys. Chem.* **1993**, *97*, 13647–13652. [CrossRef]
100. Zhao, R.; Gao, D.; Pan, X.; Xia, W.; Yu, H.; Yu, S.; Yao, L. Theoretical studies of anharmonic effect on the main reactions involving in NO_2 in fuel burning. *Chem. Phys. Lett.* **2018**, *703*, 97–105. [CrossRef]
101. Kaufman, F.; Kelso, J.R. Reaction between Nitric and Nitrous Oxide. *J. Chem. Phys.* **1955**, *23*, 602–603. [CrossRef]
102. Fishburne, E.S.; Edse, R. Shock-Tube Study of Nitrous Oxide Decomposition. *J. Chem. Phys.* **1964**, *41*, 1297–1304. [CrossRef]
103. Mebel, A.M.; Lin, M.C.; Morokuma, K.; Melius, C.F. Theoretical study of reactions of N_2O with NO and OH radicals. *Int. J. Chem. Kinet.* **1996**, *28*, 693–703. [CrossRef]
104. Hanson, R.K.; Salimian, S. Survey of Rate Constants in the N/H/O System. In *Combustion Chemistry*; Gardiner, W.C., Ed.; Springer: New York, NY, USA, 1984; pp. 361–421.
105. Ashmore, P.G.; Burnett, M.G.; Tyler, B.J. Reaction of nitric oxide and oxygen. *Trans. Faraday Soc.* **1962**, *58*, 685–691. [CrossRef]
106. Greig, J.D.; Hall, P.G. Thermal oxidation of nitric oxide at low concentrations. *Trans. Faraday Soc.* **1967**, *63*, 655–661. [CrossRef]
107. Tipper, C.F.H.; Williams, R.K. The effect of sulphur dioxide on the combustion of some inorganic compounds. Part 2. The nitric oxide+sulphur dioxide+oxygen system. *Trans. Faraday Soc.* **1961**, *57*, 79–86. [CrossRef]
108. Park, J.; Giles, N.D.; Moore, J.; Lin, M.C. A Comprehensive Kinetic Study of Thermal Reduction of NO_2 by H_2. *J. Phys. Chem. A* **1998**, *102*, 10099–10105. [CrossRef]

109. Röhrig, M.; Petersen, E.L.; Davidson, D.F.; Hanson, R.K. A shock tube study of the pyrolysis of NO_2. *Int. J. Chem. Kinet.* **1997**, *29*, 483–493. [CrossRef]
110. Zimet, E. Thermal Decomposition of N_2O_4 and NO_2 by Shock Waves. *J. Chem. Phys.* **1970**, *53*, 515–518. [CrossRef]
111. Konnov, A.A.; Ruyck, J.D. Kinetic Modeling of Nitrogen Oxides Decomposition at Flame Temperatures. *Combust. Sci. Technol.* **1999**, *149*, 53–78. [CrossRef]
112. Stagni, A.; Cavallotti, C.; Arunthanayothin, S.; Song, Y.; Herbinet, O.; Battin-Leclerc, F. An experimental, theoretical and kinetic-modeling study of the gas-phase oxidation of ammonia. *React. Chem. Eng.* **2020**, *5*, 696–711. [CrossRef]
113. Tsang, W.; Herron, J.T. Chemical Kinetic Data Base for Propellant Combustion I. Reactions Involving NO, NO_2, HNO, HNO_2, HCN and N_2O. *J. Phys. Chem. Ref. Data* **1991**, *20*, 609–663. [CrossRef]
114. Baulch, D.L.; Drysdale, D.D.; Home, D.G. *Evaluated Kinetic Data for High Temperature Reactions Vol. 2, Homogeneous Gas Phase Reactions of the H_2-N_2-O_2 System*; Butterworths: London, UK, 1973.
115. Brown, F.B.; Crist, R.H. Further Studies on the Oxidation of Nitric Oxide; the Rate of the Reaction between Carbon Monoxide and Nitrogen Dioxide. *J. Chem. Phys.* **1941**, *9*, 840–846. [CrossRef]
116. Treacy, J.C.; Daniels, F. Kinetic Study of the Oxidation of Nitric Oxide with Oxygen in the Pressure Range 1 to 20 Mm.1. *J. Am. Chem. Soc.* **1955**, *77*, 2033–2036. [CrossRef]
117. Neyrolles, E.; Lara Cruz, J.; Bassil, G.; Contamine, F.; Cezac, P.; Arpentinier, P. Kinetic study of the nitric oxide oxidation between 288 and 323 K, under pressure, focus on the oxygen influence on the reaction rate constant. *Int. J. Chem. Kinet.* **2020**, *52*, 329–340. [CrossRef]
118. Šolc, M. Kinetics of the Reaction of Nitric Oxide with Molecular Oxygen. *Nature* **1966**, *209*, 706. [CrossRef]
119. Chakraborty, D.; Park, J.; Lin, M.C. Theoretical study of the OH+NO_2 reaction: Formation of nitric acid and the hydroperoxyl radical. *Chem. Phys.* **1998**, *231*, 39–49. [CrossRef]
120. Howard, C.J. Kinetic study of the equilibrium HO_2 + NO = OH + NO_2 and the thermochemistry of HO_2. *J. Am. Chem. Soc.* **1980**, *102*, 6937–6941. [CrossRef]
121. Howard, C.J. Temperature dependence of the reaction HO_2 + NO → OH + NO_2. *J. Chem. Phys.* **1979**, *71*, 2352–2359. [CrossRef]
122. Bardwell, M.W.; Bacak, A.; Teresa-Raventos, M.; Percival, C.J.; Sanchez-Reyna, G.; Shallcross, D.E. Kinetics of the HO_2 + NO reaction: A temperature and pressure dependence study using chemical ionisation mass spectrometry. *Phys. Chem. Chem. Phys.* **2003**, *5*, 2381–2385. [CrossRef]
123. Wu, H.; Sun, W.; Huang, Z.; Zhang, Y. Biphasic sensitization effect of NO_2 on n-C4H10 auto-ignition. *Combust. Flame* **2022**, *237*, 111844. [CrossRef]
124. Gao, Z.; Yang, M.; Tang, C.; Yang, F.; Yang, K.; Deng, F.; Huang, Z. Measurements of the High Temperature Ignition Delay Times and Kinetic Modeling Study on Oxidation of Nitromethane. *Combust. Sci. Technol.* **2019**, *192*, 313–334. [CrossRef]
125. Chai, J.; Goldsmith, C.F. Rate coefficients for fuel + NO_2: Predictive kinetics for HONO and HNO_2 formation. *Proc. Combust. Inst.* **2017**, *36*, 617–626. [CrossRef]
126. Thomas, J.H. Gas phase reactions of nitrogen dioxide. Part 1.-Oxidation of acetylene. *Trans. Faraday Soc.* **1952**, *48*, 1142–1149. [CrossRef]
127. Sprung, J.L.; Akimoto, H.; Pitts, J.N., Jr. Nitrogen dioxide catalyzed geometric isomerization of olefins. Isomerization kinetics of the 2-butenes and 2-pentenes. *J. Am. Chem. Soc.* **1974**, *96*, 6549–6554. [CrossRef]
128. Parmon, V.N.; Panov, G.I.; Uriarte, A.; Noskov, A.S. Nitrous oxide in oxidation chemistry and catalysis: Application and production. *Catal. Today* **2005**, *100*, 115–131. [CrossRef]
129. Bridson-Jones, F.S.; Buckley, G.D.; Cross, L.H.; Driver, A.P. Oxidation of organic compounds by nitrous oxide. Part I. *J. Chem. Soc.* **1951**, *666*, 2999–3008. [CrossRef]
130. Bridson-Jones, F.S.; Buckley, G.D. Oxidation of organic compounds by nitrous oxide. Part II. Tri- and tetra-substituted ethylenes. *J. Chem. Soc.* **1951**, *667*, 3009–3016. [CrossRef]
131. Avdeev, V.I.; Ruzankin, S.F.; Zhidomirov, G.M. Molecular mechanism of direct alkene oxidation with nitrous oxide: DFT analysis. *Kinet Catal.* **2005**, *46*, 177–188. [CrossRef]
132. Panov, G.I.; Dubkov, K.A.; Starokon, E.V.; Parmon, V.N. Non-catalytic liquid phase oxidation of alkenes with nitrous oxide. 1. Oxidation of cyclohexene to cyclohexanone. *React. Kinet. Catal. Lett.* **2002**, *76*, 401–406. [CrossRef]
133. Dubkov, K.A.; Panov, G.I.; Starokon, E.V. Non-catalytic liquid phase oxidation of alkenes with nitrous oxide. 2. Oxidation of cyclopentene to cyclopentanone. *React. Kinet. Catal. Lett.* **2002**, *77*, 197–205. [CrossRef]
134. Karami, F.; Vahedpour, M. Theoretical study on the gas phase reaction mechanism of acetylene with nitrous oxide. *Struct. Chem.* **2012**, *24*, 1513–1526. [CrossRef]
135. Ess, D.H.; Houk, K.N. Activation Energies of Pericyclic Reactions: Performance of DFT, MP2, and CBS-QB3 Methods for the Prediction of Activation Barriers and Reaction Energetics of 1,3-Dipolar Cycloadditions, and Revised Activation Enthalpies for a Standard Set of Hydrocarbon Pericyclic Reactions. *J. Phys. Chem. A* **2005**, *109*, 9542–9553.
136. Grimme, S.; Mück-Lichtenfeld, C.; Würthwein, E.-U.; Ehlers, A.W.; Goumans, T.P.M.; Lammertsma, K. Consistent Theoretical Description of 1,3-Dipolar Cycloaddition Reactions. *J. Phys. Chem. A* **2006**, *110*, 2583–2586. [CrossRef]
137. Liu, Y.; Li, J. Quantitative Dynamics of the N_2O + C_2H_2 = Oxadiazole Reaction: A Model for 1,3-Dipolar Cycloadditions. *ACS Omega* **2020**, *5*, 23343–23350. [CrossRef]

138. Li, Y.; Jiang, R.; Xu, S.; Gong, X. Theoretical Study on the Gas-Phase Oxidation Mechanism of Ethylene by Nitrous Oxide. Propellants Explos. *Propellants Explos. Pyrotech.* **2022**, *47*, e202200082. [CrossRef]
139. Atkinson, R.; Baulch, D.L.; Cox, R.A.; Crowley, J.N.; Hampson, R.F.; Hynes, R.G.; Jenkin, M.E.; Rossi, M.J.; Troe, J. Evaluated kinetic and photochemical data for atmospheric chemistry: Volume II—Gas phase reactions of organic species. *Atmos. Chem. Phys.* **2006**, *6*, 3625–4055. [CrossRef]
140. Maricq, M.M.; Szente, J.J. Kinetics of the Reaction between Ethylperoxy Radicals and Nitric Oxide. *J. Phys. Chem.* **1996**, *100*, 12374–12379. [CrossRef]
141. Chow, J.M.; Miller, A.M.; Elrod, M.J. Kinetics of the $C_3H_7O_2$ + NO Reaction: Temperature Dependence of the Overall Rate Constant and the i-$C_3H_7ONO_2$ Branching Channel. *J. Phys. Chem. A* **2003**, *107*, 3040–3047. [CrossRef]
142. Butkovskaya, N.I.; Kukui, A.; Bras, L.G.; Rayez, M.T.; Rayez, J.C. Pressure Dependence of Butyl Nitrate Formation in the Reaction of Butylperoxy Radicals with Nitrogen Oxide. *J. Phys. Chem. A* **2015**, *119*, 4408–4417. [CrossRef]
143. Cassanelli, P.; Fox, D.J.; Cox, R.A. Temperature dependence of pentyl nitrate formation from the reaction of pentyl peroxy radicals with NO. *Phys. Chem. Chem. Phys.* **2007**, *9*, 4332–4337. [CrossRef]
144. Atkinson, R.; Aschmann, S.M.; Winer, A.M. Alkyl nitrate formation from the reaction of a series of branched RO_2 radicals with NO as a function of temperature and pressure. *J. Atmos Chem.* **1987**, *5*, 91–102. [CrossRef]
145. Eberhard, J.; Howard, C.J. Rate Coefficients for the Reactions of Some C_3 to C_5 Hydrocarbon Peroxy Radicals with NO. *J. Phys. Chem. A* **1997**, *101*, 3360–3366. [CrossRef]
146. Feng, B.; Sun, C.; Zhang, S. Atmospheric degradation mechanism of benzyl peroxy radical: A theoretical study. *Atmos Env.* **2019**, *201*, 18–27. [CrossRef]